

# We are IntechOpen, the world's leading publisher of Open Access books Built by scientists, for scientists

6,900

Open access books available

186,000

International authors and editors

200M

Downloads

Our authors are among the

154

Countries delivered to

TOP 1%

most cited scientists

12.2%

Contributors from top 500 universities



WEB OF SCIENCE™

Selection of our books indexed in the Book Citation Index  
in Web of Science™ Core Collection (BKCI)

Interested in publishing with us?  
Contact [book.department@intechopen.com](mailto:book.department@intechopen.com)

Numbers displayed above are based on latest data collected.  
For more information visit [www.intechopen.com](http://www.intechopen.com)



---

# Radiologic Assessment of Liver Fibrosis – Present and Future

---

Luca Macarini and Luca P. Stoppino

Additional information is available at the end of the chapter

<http://dx.doi.org/10.5772/55164>

---

## 1. Introduction

Liver fibrosis results from chronic damage to the liver in conjunction with the accumulation of extracellular matrix (ECM) proteins including collagen, which is a characteristic of most types of chronic liver diseases (CLD) [1]. Hepatic fibrosis was historically thought to be a passive and irreversible process due to the collapse of the hepatic parenchyma and its substitution with a collagen-rich tissue [2, 3]. Currently, is recognised to be a dynamic process that can progress or regress over periods as short as months [4].

This process is associated with an inflammatory response and a limited deposition of ECM. If the hepatic injury persists, then eventually the liver regeneration fails, and hepatocytes are substituted with abundant ECM. The distribution of this fibrous material depends on the origin of the liver injury. In chronic viral hepatitis and chronic cholestatic disorders, the fibrotic tissue is initially located around portal tracts, while in alcohol-induced liver disease, it locates in pericentral and perisinusoidal areas [5]. As fibrotic liver diseases advance, the hepatic architecture is distorted by the accumulation of ECM proteins leading to the formation of a fibrous scar and the subsequent development of nodules of regenerating hepatocytes defines cirrhosis. Main event in this process is the activation of the hepatic stellate cells, the main collagen-producing cells, by fibrogenic cytokines. Other cells such as portal fibroblasts and bone marrow-derived cells may also be involved in the fibrogenic process [1].

Liver biopsy is considered the current clinical standard of reference for the assessment of liver fibrosis [6]. Histologic examination is useful in identifying the underlying cause of liver disease and assessing the necro-inflammatory grade and the stage of fibrosis. However, it represents an invasive procedure, with pain and major complications occurring in 40% and 0.5% of patients, respectively [7]. Further, liver biopsy can be associated with substantial sampling-error. Histologic examination is subject to intra- and inter-observer variation and does not

predict disease progression [8]. Therefore, there is a need for reliable, simple, and non-invasive methods for assessing liver fibrosis. In recent years, a wide variety of imaging-based methods have been used for noninvasively assessing liver fibrosis, including ultrasound, CT and MRI.

In this chapter, we provide an overview of the newer imaging techniques used in the evaluation of liver fibrosis.

## 2. Epidemiology and natural history

Fibrosis leading to cirrhosis can accompany virtually any CLD that is characterized by the presence of architectural disruption and/or inflammation. Over many years the principle causes of CLD have been chronic viral hepatitis B and alcoholic liver disease. Other etiologies of liver disease include parasitic infestation (e.g. schistosomiasis), autoimmune attack on hepatocytes or biliary epithelium, neonatal liver disease, metabolic disorders including Wilson's disease, hemochromatosis and a variety of storage diseases, chronic inflammatory conditions (e.g. sarcoidosis), drug toxicity (e.g. methotrexate or hypervitaminosis A), and vascular derangements, either congenital or acquired. While rates of alcoholism and alcoholic liver disease are falling in many countries, hazardous drinking amongst young people is resulting in alarming rates of alcoholic liver disease in several northern European countries [9, 10]. Over the last few decades two other diseases have emerged to make a major contribution to the burden of CLD. Chronic hepatitis C and non-alcoholic fatty liver disease (NAFLD) are recognised to have already had a major impact on CLD incidence. Hepatitis C virus (HCV) is transmitted in blood and blood products through unsafe injection practices and the therapeutic use of infected blood products. It is thought that the world prevalence of chronic hepatitis C is nearly 200 million people [11, 12]. In the developed world with rapidly increasing rates of obesity, NAFLD is considered to represent a major cause of significant fibrosis. Although it appears that only a minority of patients with NAFLD (maybe 20%) develop significant fibrosis, due to the vast prevalence of the at-risk overweight population, NAFLD may give rise to an epidemic of liver fibrosis [13, 14].

Of the many causes of CLD, our understanding of natural history of fibrosis is most complete in HCV, with some information about HBV and steatohepatic diseases, including alcoholic liver disease and NAFLD. Fibrosis associated with HCV can assume a variable course, from decades of viremia with tiny fibrosis to a rapid onset of cirrhosis within 10–15 years. It appears to be host factors rather than viral factors that correlate with fibrosis progression in HCV, such as older age at the time of infection, concurrent liver disease due to HBV or alcohol (>50g/day), male gender, increased body mass index (BMI) and HIV infection or immunosuppression [15, 16].

Information about fibrosis progression in other diseases is largely subjective, but the development of cirrhosis typically requires many years to decades. There are, however, some notable exceptions in which the development of cirrhosis can be greatly accelerated, possibly occurring within months rather than years: (1) neonatal liver disease – infants with biliary atresia may present at birth with severe fibrosis and marked parenchymal distortion; (2) HCV-infected patients after liver transplantation – a subset of patients who undergo liver trans-

plantation for HCV cirrhosis may develop rapidly progressive cholestasis and recurrent cirrhosis within months, requiring retransplantation [17]; (3) patients with HIV/HCV co-infection – these patients have relatively rapid fibrosis compared to those with HCV alone [18], especially if the HIV is untreated; (4) severe delta hepatitis [19]; and (5) some cases of drug-induced liver disease. These examples of ‘fulminant fibrosis’ probably reflect dysregulation of several pathways, including defective immunity, massive inflammation and necrosis, and/or altered matrix resorption.

### 3. Assessment of stage of fibrosis

Liver biopsy is a common element of diagnostic workup in hepatic cirrhosis, and is the accepted diagnostic gold standard. Several systems for scoring liver fibrosis have been proposed in order to classify the progression of fibrosis to cirrhosis into discrete stages, each based on visual assessment of collagen staining of liver biopsy samples. The more frequently used systems are the histology activity index (HAI: Knodell score) [20], the Ishak modification of the HAI score [21], and the Metavir score [22].

The HAI system consists of the evaluation of two histopathological categories, necroinflammation and fibrosis. Furthermore, necroinflammation includes three subcategories: periportal necrosis and inflammation, scored from 0 to 10; intralobular necrosis and inflammation, scored from 0 to 4; and portal inflammation, scored from 0 to 4. Fibrosis is scored as 0, 1, 3, or 4, with 1 indicating portal fibrosis only, 3 indicating bridging fibrosis, and 4 indicating cirrhosis. The HAI score is the combined scores for necrosis, inflammation, and fibrosis, while the overall HAI scores can also be broken into individual components of necrosis, inflammation, and fibrosis to yield additional information [20]. Despite this system is widely used, is relatively insensitive to changes in fibrosis (lack of a score for stages between mild and severe), and has an intra- and inter-observer reproducibility relatively poor.

Ishak et al. [21] have proposed a modification of the HAI scoring system, which uses similar scores for necroinflammatory changes (activity: 0 to 18), but scores fibrosis on a scale from 0 to 6. Scores of 1 and 2 indicate portal fibrosis, 3 and 4 bridging fibrosis, 5 incomplete or early cirrhosis, and 6 established cirrhosis. The Ishak scale provides better discrimination in assessing small changes in fibrosis, permitting a better assessment of progression of disease, and possible effects of therapy. The intra- and interobserver variability of the Ishak scoring system has yet to be carefully defined.

The Metavir score [22] was developed in an attempt to address some of the problems with the Knodell score. The Metavir score is a semiquantitative classifications system and scores both necroinflammatory changes that fibrosis. The activity score is graded according to the intensity of necroinflammatory lesions (A0 = no activity, A1 = mild activity, A2 = moderate activity, A3 = severe activity). The fibrosis score is assessed on a five point scale (F0 = no fibrosis, F1 = portal fibrosis without septa, F2 = few septa, F3 = numerous septa without cirrhosis, F4 = cirrhosis) (Figure 1). Clinically significant fibrosis is generally defined by F2 involvement or greater. Compared to the Knodell fibrosis score (which has only four levels), the Metavir score permits

recognition of subtler variation in the degree of fibrosis. The Metavir system has been carefully validated and shows good intra- and interobserver reproducibility. This system is commonly used in Europe. Table 1 compares the three systems described for evaluating the stage of fibrosis.

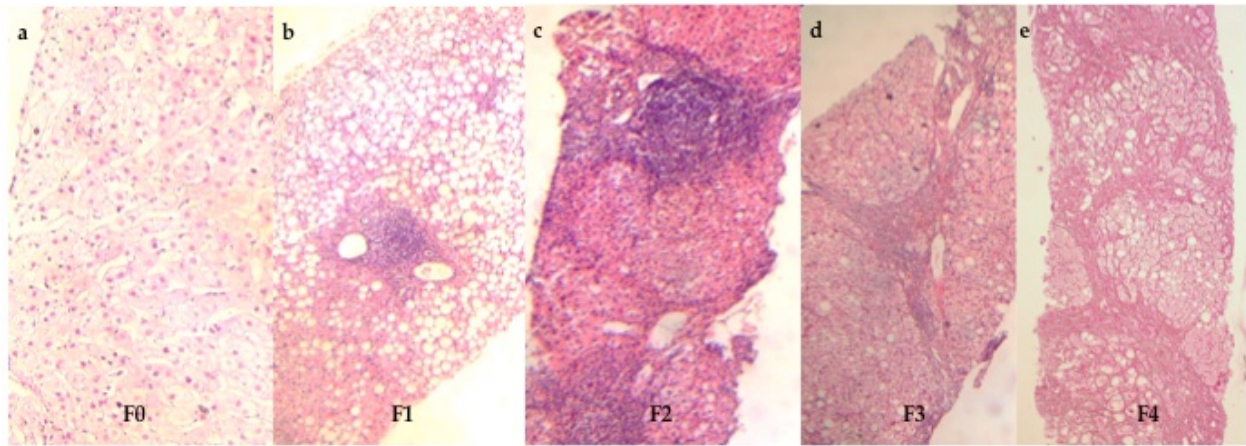


**Figure 1.** Progression of fibrosis from periportal fibrosis to cirrhosis according to the Metavir scoring system shown through photomicrographs (original magnification,  $\times 10$ ; Hematoxylin and Eosin stains) of histologic sections from liver biopsy specimens. **(a)** No fibrosis (stage F0). **(b)** Portal and periportal fibrosis only (stage F1). **(c)** Periportal fibrosis with few septa (stage F2). **(d)** Septal fibrosis and bridging without cirrhosis (stage F3). **(e)** Cirrhosis (stage F4) which appears as nodules of liver parenchyma separated by thick fibrous bands.

| Stage of fibrosis | HAI (Knodell)                     | Ishak   | Metavir*                             |
|-------------------|-----------------------------------|---|--------------------------------------|
| 0                 | No fibrosis                       | No fibrosis   | No fibrosis                          |
| 1                 | Portal fibrosis                   | Fibrosis of isolated portal areas with or without short septa   | Portal fibrosis                      |
| 2                 | n. d.                             | Increased fibrosis in most portal areas with or without short septa                                     | Portal fibrosis with scattered septa |
| 3                 | Portoportal or portocentral septa | Portal fibrosis with portoportal septa  | Numerous septa without cirrhosis     |
| 4                 | Cirrhosis                         | Portal fibrosis Cirrhosis with marked portoportal or portocentral septa                                 | Cirrhosis                            |
| 5                 | n. d.                             | Marked septum formation (portoportal or portocentral) with some nodule formation (incomplete cirrhosis) |                                      |
| 6                 | n. d.                             | Probable or definite cirrhosis  | n. d.                                |

n. d. = not defined;

\* only validated in chronic hepatitis C

**Table 1.** Histological classification systems for evaluating the stage of fibrosis

According to the average size of the parenchymal nodules, *cirrhosis* may be classified into micronodular, macronodular, and mixed types. While micronodular cirrhosis is defined as nodules less than 0.3 cm in diameter, macronodular cirrhosis is defined as nodules larger than 0.3 cm. Micronodular cirrhosis is generally caused by diffuse liver injury, such as alcohol, other hepatotoxic agents, and metabolic disorders (nonalcoholic steatohepatitis), whereas macronodular cirrhosis is observed in disease processes where hepatocellular regeneration plays a significant role (chronic and autoimmune hepatitis) [23].

Although the scoring systems mentioned above for hepatic fibrosis are extremely useful in diagnosis and staging of liver fibrosis, all of these systems have important limitations. Hepatic fibrosis may not be homogenous throughout the liver, and the liver specimen obtained by the needle biopsy may not accurately reflect the overall average degree of fibrosis. A number of studies have demonstrated excessive rates of sampling error (25%-40%) resulting in poor reproducibility regardless of underlying liver disease origin [24]. The extent of variation from observer interpretation by expert histopathologists may be as high as 20% [25]. In addition, there is mounting evidence that liver biopsy has a number of limitations for its use in these roles as well. These include: (a) the effect of reduced biopsy size (<25 mm) and complete portal tract number (<11) on understaging fibrosis; (b) interobserver variation in histological interpretation; and (c) the qualitative nature of assessing fibrosis in 2 dimensions with descriptive staining techniques. Ultimately, the method of percutaneous liver biopsy is an invasive procedure with poor acceptance by patients. The associated morbidity from this technique is estimated at 3% with a mortality rate of 0.03% [26].

In summary, although liver biopsy is considered the standard of reference, it has several limitations (invasiveness, complications, sampling variability, subjectivity) that restrict its role as a method for screening and longitudinal assessment of liver fibrosis. New reproducible and reliable noninvasive techniques are required to evaluate disease progression in patients with CLD, and to monitor pharmacological treatment.

#### 4. Imaging techniques

Since morphologic alterations and features of portal hypertension are present only in advanced CLD, routine examinations by ultrasound (US), computed tomography (CT) and magnetic resonance imaging (MRI) could produce specific findings, but with very limited sensitivity. The ability to detect early and intermediate stages of fibrosis using conventional ultrasound with Doppler assessment of the hepatic vasculature is unsatisfactory [27]. CT offers improved resolution of early morphological changes with cirrhosis but has low accuracy in fibrosis detection [28]. In fact, quantitative assessment of the density distribution of liver parenchyma showed that only diffuse steatosis and active alcoholic cirrhosis had significantly different mean hepatic attenuation values [29]. Moreover, most studies of contrast-enhanced CT involved patients with cirrhosis [30, 31] and it is thus unclear if changes in hepatic enhancement could be used to diagnose mild or moderate hepatic fibrosis. MRI identify specific features of cirrhosis such as hepatic vein narrowing, caudate to right lobe ratio, and expanded gallbladder

fossa [32], but remains lacking in earlier stages of fibrosis [33]. Hence, assiduous efforts have been made to search for technological developments.

#### 4.1. Sonography-based techniques for assessment of liver fibrosis

Recently, diverse sonography-based techniques have been used in assessment of liver fibrosis, including Transient Elastography, Real-Time Elastography, and Acoustic Radiation Force Imaging sonoelastography.

**Transient Elastography.** Transient Elastography (TE) (FibroScan®, Echosens, Paris, France) is a new imaging modality for detecting hepatic fibrosis. The measuring instrument comprises a computer driven control unit and a probe with an ultrasound transducer, which is located at the end of a vibrating piston. The piston generates a low frequency elastic wave (5 Mhz) that passes through the skin and liver tissue and is transmitted into hepatic tissue at a speed of around 1 m/s. The ultrasound then detects the propagation of the shear wave through the liver by measuring its velocity. The shear wave velocity is directly related to the tissue stiffness, with a higher velocity equating to higher tissue stiffness, corresponding to increasing severity of fibrosis.

TE is carried out with the patient supine, with his/her right arm behind their head. The measuring probe is positioned at the level of the xiphoid in the right mid-axillary line, at 90 degrees to the body. TE measures liver stiffness in a volume that approximates a cylinder 1 cm wide and 4 cm long, between 2,5 cm and 6,5 cm below the skin surface (Figure 2). Ten validated measurements are required, with the median value taken as the final result, which is expressed in units of kilopascals (kPa). The range of possible liver stiffness values obtained with this technique is from 2.5 to 75.0 kPa, with the normal liver stiffness value for healthy individuals being around 5.5 kPa (Figure 3) [34].

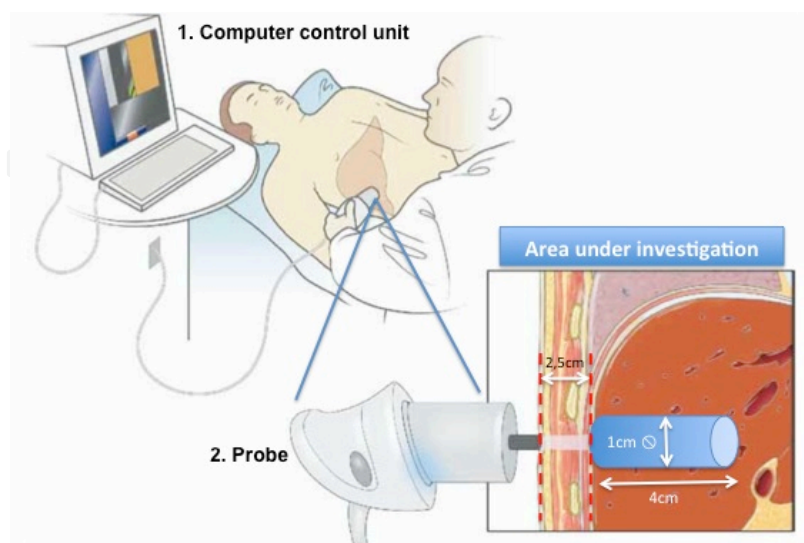


**Figure 2.** Illustration of the two different constituent of the measuring instrument and the positioning of the probe in relation to the area of liver under investigation.

The advantages of TE are that the results are immediately available, and the procedure is painless, rapid (~3 minutes per patient), and easy to perform. The interequipment, intraobserver (96–98%) and interobserver agreement (89–98%) of TE has been shown to be excellent, but the success rate depends on observer expertise, patient BMI and intercostal space [35–37]. Moreover, TE is a reliable method for the diagnosis of extensive fibrosis (Metavir F=3) and cirrhosis (F=4): positive and negative predictive values range from 70–95% and 77–95%, respectively [38–41]. The age of the subject does not affect liver stiffness, and males tend to have a slightly higher liver stiffness value compared to females [34]. One of the important aspects of liver stiffness measurements is the cut-off values that are adopted for different stages of fibrosis, with higher cut-off levels corresponding to higher fibrosis stages.

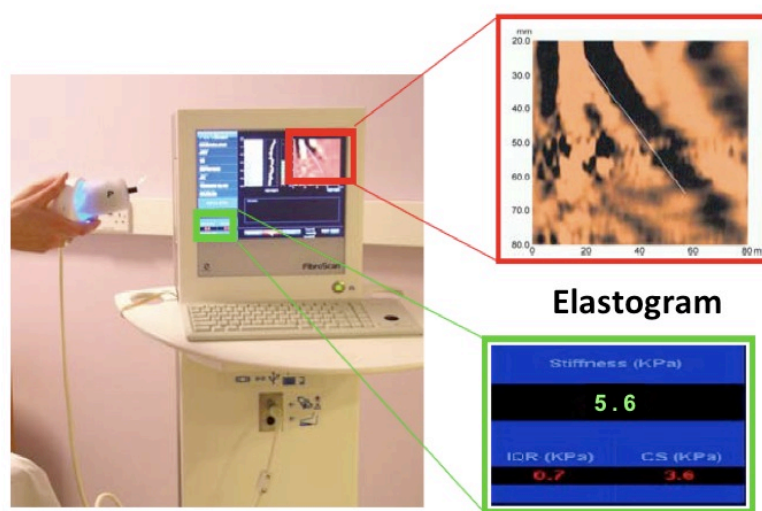


**Figure 3.** Example of shear wave propagation velocity in healthy subject with normal liver stiffness.

The cut-off levels are also different for different diseases. Therefore it is important to interpret the results with the cut-off values specific for the underlying condition. Table 2 show a summary of the cut-off values used for specific liver diseases. For example, in HCV patients according to Castera et al. [42], liver stiffness cut-off values were 7.1 kPa for F $\geq$ 2, 9.5 kPa for F $\geq$ 3, and values  $\geq$  12.5 kPa for F=4 (defined according to Metavir system).

There are some physical limitations of TE, such as obesity (particularly the fatness of the chest wall), narrow intercostal space and ascites. Moreover, Fraquelli et al. found that TE reproducibility is significantly reduced in patients with steatosis, an increased BMI and lower degrees of hepatic fibrosis [35]. TE is an innovative and user-friendly technology for the assessment of hepatic fibrosis in patients with CLD. However, despite strong academic and commercial promotion, the key reason that TE cannot completely substitute a liver biopsy is that it is unable to diagnose liver disease and it only allows staging with the best diagnostic performances for severe fibrosis and cirrhosis. Assessment of pre-cirrhotic disease and the longitudinal assessment of change in fibrosis have not been fully evaluated.

| Author                   | Disease                | Cut-off F $\geq$ 2<br>(kPa) | Cut-off F $\geq$ 3<br>(kPa) | Cut-off F=4<br>(kPa) | Results   |
|--------------------------|------------------------|-----------------------------|-----------------------------|----------------------|---|
| Castera et al. [42]      | HCV                    | 7.1                         | 9.5                         | 12.5                 | AUROC for F $\geq$ 2: 0.80<br>AUROC for F $\geq$ 3: 0.90<br>AUROC for F=4: 0.95 |
| Marcellin et al. [43]    | HBV                    | 7.2                         | 8.1                         | 11.0                 | AUROC for F $\geq$ 2: 0.81<br>AUROC for F $\geq$ 3: 0.93<br>AUROC for F=4: 0.93 |
| de Ledinghen et al. [44] | HIV/HCV<br>coinfection | 4.5                         | n.d.                        | 11.8                 | AUROC for F $\geq$ 2: 0.72<br>AUROC for F=4: 0.97                               |
| Yoneda M et al. [45]     | NAFLD                  | 6.6                         | 9.8                         | 17.5                 | AUROC for F $\geq$ 2: 0.87<br>AUROC for F $\geq$ 3: 0.90<br>AUROC for F=4: 0.99 |
| Corpechot C et al. [46]  | PBC or PSC             | 7.3                         | 9.8                         | 17.3                 | AUROC for F $\geq$ 2: 0.92<br>AUROC for F $\geq$ 3: 0.95<br>AUROC for F=4: 0.96 |

n. d. = not defined; PBC = primary biliary cirrhosis; PSC = primary sclerosing cholangitis.

**Table 2.** Diagnostic performance of TE for the diagnosis of cirrhosis according to liver disease

**Real-Time Elastography.** Real-Time Elastography (RTE) is an alternative method for measurement of tissue elasticity integrated in a sonography machine developed by Hitachi Medical Systems. This technique can reveal the physical property of tissue using conventional ultrasound probes during a routine sonography examination. Ophir et al. [47] first described the principle of this technique in 1991. To reduce the time-consuming calculations, Pesavento et al. [48] developed a fast cross-correlation technique that is the basis for RTE. The difference in hardness between diseased and surrounding tissue can be detected by RTE based on the physical properties of the tissue [49, 50]. In effect, this method measures the degree of tissue distortion (strain), mechanically induced, in the B mode image to quantify the elasticity of the tissue. By measuring the tissue strain induced by compression, it is possible to estimate the tissue hardness. The calculation of tissue elasticity distribution is assessed in real-time ultrasound imaging and depicted as color-coded images with the conventional B-mode image in the background [49, 51]. The color scale includes the following colors: red (soft tissue), green (intermediate, normal tissue), and blue (anelastic, hard tissue).

RTE is carried out with patients in a supine position with the right arm elevated above the head. Breathing does not cause any motion artifacts since each elastography image is obtained in a few milliseconds. The examination is performed on the right lobe of the liver through the intercostal space. 5-9 MHz probe is used because higher frequencies allow better analysis of areas close to the transducer. The measurement depth is between 20 and 50 mm (mean, 35 mm) with a 350–500 mm<sup>2</sup> area of measurement. The results are considered consistent only applying a pressure of

3–4 on a scale of 0–6 arbitrary units (Figure 4). Ten valid measurements are performed in each subject and the entire examination lasts approximately 5–10 minutes per patient.

Friedrich-Rust et al. first assessed real-time elastography for the detection of liver fibrosis [52], founding that the area under the receiver operating characteristic (AUROC), a measurement of the diagnostic accuracy of a test, was 0.75 for the diagnosis of significant fibrosis ( $F \geq 2$ ). A significant increase in accuracy (AUROC = 0.93) was obtained by combining RTE score and two routine laboratory values (platelet count and GGT). In a recent paper Wang et al. [53] compared the overall elasticity determined by RTE in 55 patients with liver fibrosis and chronic hepatitis B and in 20 healthy volunteers. Using a new quantitative technology for diffuse histological lesion with 11 parameters characterizing the stiffness degree of tissue, the AUROC was 0.93 ( $F \geq 1$ ,  $p < 0.001$ ) for the diagnosis of liver fibrosis, 0.92 ( $F \geq 2$ ,  $p < 0.001$ ), 0.84 ( $F \geq 3$ ,  $p < 0.05$ ) and 0.66 ( $F = 4$ ,  $p > 0.05$ ), respectively.

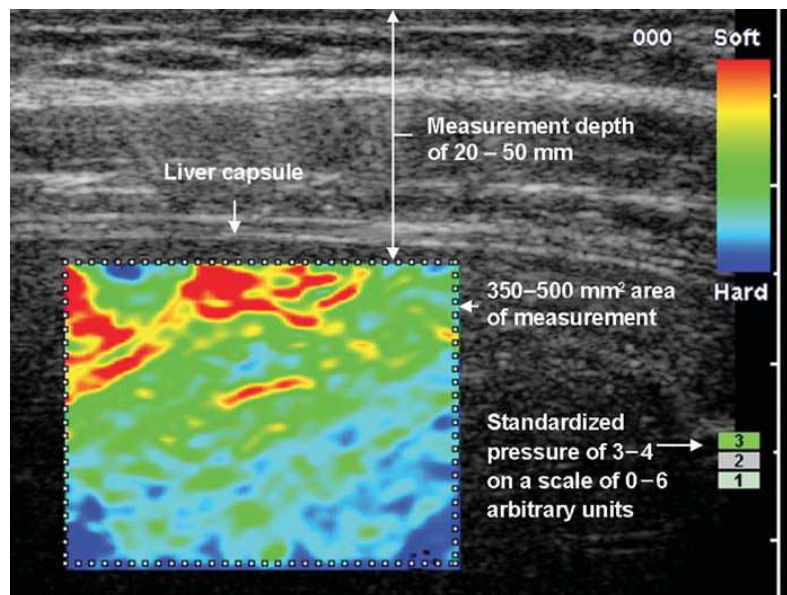


**Figure 4.** Example of tissue elasticity distribution in a healthy subject represented as color-coded images over conventional B-mode image.

As for TE even for RTE obesity, narrow intercostal space and ascites are potential physical limitations. More number of sample about chronic hepatitis with assessment by RTE is needed to performed to certify its advantages.

**Acoustic Radiation Force Impulse Elastography.** Acoustic Radiation Force Impulse (ARFI) imaging is a novel ultrasound-based elastography method that is integrated in a conventional ultrasound machine enabling the exact localization of measurement site. ARFI imaging involves the mechanical excitation of tissue using short-duration acoustic pulses ( $\approx 262 \mu\text{sec}$ ) with a fixed transmit frequency of 2.67 MHz to generate localized, micron-scale displacements in tissue. The first available applications to implement this technology are Virtual Touch tissue imaging and Virtual Touch tissue quantification (Siemens, Erlangen, Germany). Unlike conventional B-mode sonography, which provides anatomical details based on differences in

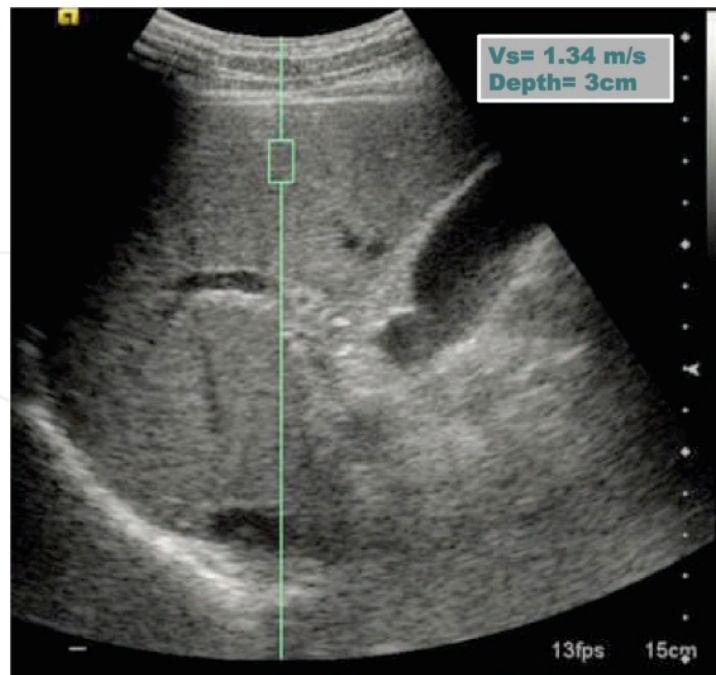


**Figure 5.** Measurement of the shear wave velocity with ARFI. The region of interest is placed 2–3 cm from the liver capsule at the right hepatic lobe, where the liver tissue is at least 5.5 cm thick.

acoustic impedance, Virtual Touch™ imaging describes relative physical tissue stiffness properties. In complement, Virtual Touch™ tissue quantification provides accurate numerical measurements related to tissue stiffness at user-defined anatomical locations. ARFI technology quantifies stiffness without manual compression since, using the Virtual Touch™ application, the tissue is compressed by acoustic energy. Virtual Touch tissue quantification is a quantitative assessment of tissue stiffness, through measurement of shear wave speed.

The system uses a standard ultrasonographic probe and offers elastography with a flexible metering box of 1 cm at variable depths (Figure 5). An acoustic push pulse transmitted by the transducer (3.5 MHz) toward the tissue induces an elastic shear wave that propagates through the tissue (Figure 6). The propagation of the shear wave is followed by detection pulses that are used to measure the velocity of shear wave propagation, which is directly related to tissue stiffness: speed increases with stiffness. The measurements were performed on the right lobe of the liver through the intercostal spaces, away from motion and portal/hepatic vessels, about 2 cm from the liver capsula, at a depth between 3.8 and 5.5 cm. Usually a total of 10 valid measurements per patient are performed. In difficult patients, to obtain better access to the liver without excessive pushing or breath holding, the measurements were performed on patients lying in the left lateral decubitus position, or using a subcostal approach to the left lobe. The results are expressed by the shear wave velocity - SWV (m/s). Thus, the measured SWV is an intrinsic and reproducible property of the tissue [54-56].

According to Sporea et al., [57] despite exhibiting a strong correlation with histological fibrosis, ARFI is an accurate test only for the prediction of severe fibrosis and cirrhosis (F=4) using 1.7 m/s as cut-off value (AUROC: 0.931, sensibility: 93%, specificity: 86.7%). Recently, a meta-

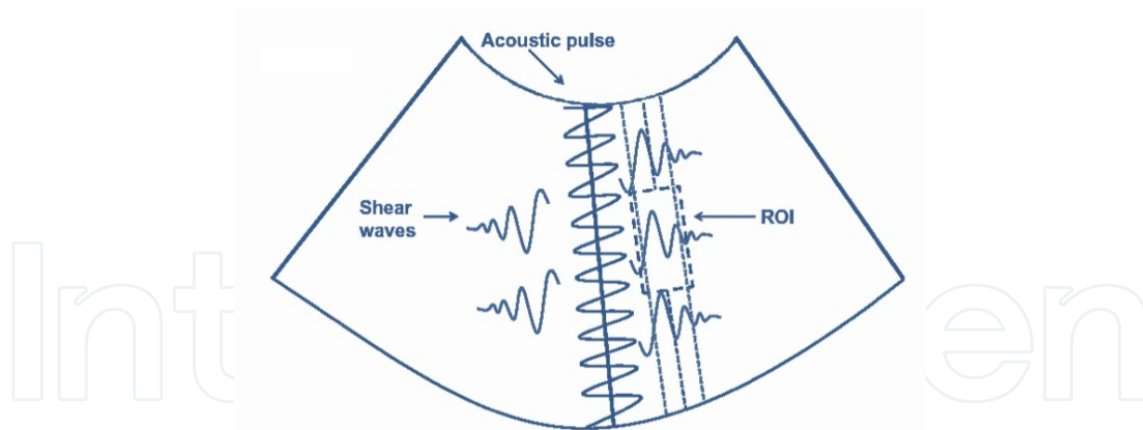


**Figure 6.** Principle of Acoustic Radiation Force Elastography. Transmission of short-duration acoustic pulses generates tissue displacement within a localized area of the liver, resulting in shear waves propagating away from the region of excitation. Shear wave velocity is measured in meters/s within a defined region of interest (ROI), and is proportional to the square root of tissue elasticity.

analysis was performed [58] including ARFI patient data obtained from eight studies for a total of 518 patients. The authors found that the AUROC was 0.87 for the diagnosis of significant fibrosis ( $F \geq 2$ ), 0.91 for the diagnosis of severe fibrosis ( $F \geq 3$ ), and 0.93 for the diagnosis of cirrhosis. The optimal cut-off for  $F \geq 2$  was 1.34 m/s, for  $F \geq 3$  1.55 m/s and for the diagnosis of liver cirrhosis 1.80 m/s, respectively.

Finally, Colombo et al. [59] performed a head-to-head comparison of TE, RTE, and ARFI imaging in the diagnosis of liver fibrosis, in a population consisting of 27 normal subjects and 54 patients with CLD. The three methods showed high correlation with fibrosis and poor correlation with necro-inflammatory activity, with TE showing the best performance (AUROC was 0.87 for  $F \geq 1$  and 0.89 for  $F \geq 2$ , with the best cut-offs set at 6.3 kPa for fibrosis and 7.8 kPa for significant fibrosis). Only TE and ARFI exhibited high diagnostic accuracy (AUROC  $\geq 0.9$ ) in diagnosing cirrhosis ( $F=4$ ). However, TE was unsuccessful in 15% of patients, mainly due to obesity. Nevertheless, the authors conclude that TE is probably the best method to screen for CLD patients in the general population and to identify significant fibrosis, but further studies are needed to fully explore the potential of RTE, since its technology and the equations used to calculate tissue elasticity are rapidly changing.

#### 4.2. MR imaging-based techniques for assessment of liver fibrosis

In the last decade, the development of MRI scanner with high-performance magnetic field gradients made the introduction of three-dimensional sequences for liver imaging possible. Volumetric image acquisitions with near-isotropic voxels (1–3 mm in all three-dimensions) through the entire liver can be achieved in a single breath-hold or using respiratory triggering. In detail, several technological advances have been made for assessment of fibrosis, including Conventional MRI, Double contrast-material enhanced MRI, Diffusion-weighted MRI, MR elastography, perfusion MRI, and MR spectroscopy.

**Unenhanced MRI.** In patients with precirrhotic stages of liver fibrosis as well as patients with early cirrhosis, the liver parenchyma usually has a normal appearance or may reveal only subtle, generic heterogeneity on unenhanced MRI [60]. Conversely, in patients with advanced cirrhosis, fibrotic septa and bridges show low-signal-intensity reticulations on T1-weighted images and high signal-intensity reticulations on T2-weighted images (Figure 7) [61]. Dodd et al. [62] described four different patterns of diffuse fibrosis detectable on T2-weighted images: (1) patchy, poorly defined regions of high signal intensity, (2) thin perilobular bands of high signal intensity, (3) thick bridging bands of high signal intensity that surround regenerative nodules, and (4) diffuse fibrosis that causes perivascular (bull's-eye) cuffing. Although most forms of diffuse fibrosis can occur in any type of cirrhosis, thin perilobular bands and perivascular cuffing appear most commonly in primary biliary cirrhosis. The large water content of advanced fibrosis provides prolonged T2 relaxation times and may explain these signal intensity characteristics [63]. These reticulations frequently enclose regenerative nodules, which are <2 cm and isointense to hyperintense on T1-weighted images, isointense to hypointense on T2-weighted images. Lipid-containing nodules or steatotic nodules display signal loss on out-of-phase gradient echo (GRE) images in comparison with in-phase images. Iron containing nodules or siderotic nodules appear markedly hypointense on T2-weighted and T2\*-weighted images [63].



**Figure 7.** Unenhanced MR imaging in a 61-year-old man with alcohol-related cirrhosis. Unenhanced T1-weighted image (a) shows hypointense reticulations (arrows) and numerous regenerative nodules (arrowheads), which are iso- to hyperintense. Unenhanced T2-weighted fat-saturated image (b) allows a clearer visualization of the reticulations throughout the liver parenchyma visible as hyperintense septa (arrows).

Fibrotic scars up to several centimetres thick characterize *confluent fibrosis* with a mass-like appearance seen in approximately 15% of patients with advanced cirrhosis. Confluent fibrosis has similar signal intensity as fibrotic septa and bridges but is easier to visualize because of its size. This mass-like fibrosis typically has a wedge-shaped area, radiates from the portal hilum, contacts and retracts the liver capsule, and causes focal volume loss.

Furthermore, the cirrhotic liver develops characteristic morphologic alterations such as surface nodularity, widening of fissures, expansion of the gallbladder fossa, notching of the right lobe, atrophy of the right lobe, and relative enlargement of the lateral segments of the left lobe and

caudate lobe (Figure 8) [62]. However, these signs of advanced disease have high specificity for cirrhosis but there are only few publications on unenhanced MRI for the staging of hepatic fibrosis.

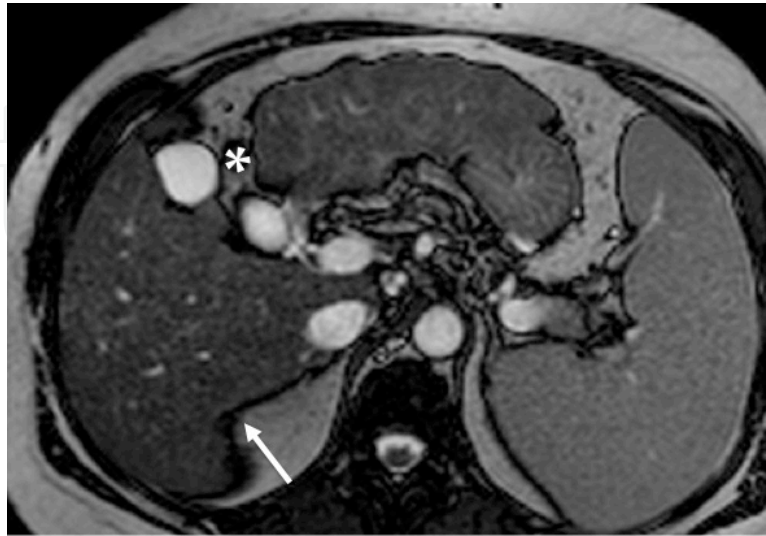


**Figure 8.** Axial Balanced fast field echo image in a 59-year-old man with alcoholic cirrhosis shows surface nodularity, hypertrophy of the left lobe, expanded gallbladder fossa (asterisk), and notching of the right lobe (arrow).

**Contrast-enhanced MRI.** The detection of liver fibrosis is improved by the administration of contrast agents. Three contrast agents are currently commercially available: gadolinium-based contrast agents; superparamagnetic iron oxide particles; Gd-EOB-DTPA.

Gadolinium-based contrast agents cause T1 shortening and signal enhancement on T1-weighted images. Most gadolinium-based contrast agent formulations freely equilibrate with the extracellular compartment and accumulate in tissues with large extracellular volumes such as liver fibrosis [64]. Thus, most gadolinium-based contrast agents preferentially enhance the signal of liver fibrosis on T1-weighted images. The reticulations enhance progressively after contrast agent administration. Although some of the reticulations are enhanced at the arterial phase, most are not enhanced until the more delayed images (late venous and equilibrium phases) (Figure 9). Similarly, the persistence of enhancement of the confluent fibrosis into the late phases associated with its characteristic morphology allows differentiation from HCC.

Superparamagnetic iron oxide particles (SPIO) are reticulo-endothelial-specific particulate MRI contrast agents which are cleared from the blood through phagocytosis and accumulate in the cells of the reticulo-endothelial system of the liver, spleen, and bone marrow, with approximately 80% taken up by the liver. SPIO markedly shorten T2 relaxation rates and signal loss is greatest with gradient recalled echoes because these are highly sensitive to T2\*-shortening effects. Consequently, the signal intensity of the liver parenchyma decreases on T2-weighted sequences, except in the areas with reduced Kupffer cell density, like fibrosis within the liver, which accumulate less iron oxide and appear as high signal-intensity reticulations (Figure 10) [65]. Two SPIO particle formulations are clinically available, namely ferumoxides and ferucarbotran. Ferumoxides (Feridex IV, Berlex Laboratories; and Endorem, Guerbet) is a

SPIO colloid with low molecular weight dextran coating, with a particle size of 120-180 nm. This contrast agent is prepared as a dilution in 100 ml of 5% dextrose and administered as a drip infusion over about 30 min. At about 8 min following the intravenous injection, iron oxide particles are taken up by the reticulo-endothelial cells in the liver and in the spleen. Maximum signal loss is obtained after 1 h with an imaging window ranging from 30 min to 6 h after the injection. The recommended dosage of Endorem (ferumoxides injectable solution) is 0.56 milligrams of iron (0.05 mL Feridex IV) per kilogram of body weight. Ferucarbotran (Resovist, Bayer Healthcare) is a carboxydextrane-coated SPIO, with a hydrodynamic diameter ranging between 45 and 60 nm. Unlike Endorem, Resovist can be safely injected rapidly in a bolus fashion, and has an effect on the shortening of both T1 and T2 relaxation time. Dynamic T1-weighted GRE 3D sequences can be performed to acquire the perfusion properties of the lesion during the arterial and portal venous phases of the contrast agent. On dynamic MR imaging using T1-weighted GRE, enhancement was positive in the liver for at least 30 s after bolus injection of SPIO. On delayed images after 10 min, the T2/T2\* effects are observed due to the reticulo-endothelial uptake in the liver. The recommended dose of Resovist is: for patients weighing less than 60 kg: 0.9 ml Resovist); for adults patients weighing 60 kg or more: 1.4 ml Resovist. Lucidarme et al. describe hypersignal intensities on the SPIO enhanced T2-weighted sequences in 76% of patients with chronic hepatitis and a Metavir score of  $F \geq 2$  with good specificity (80%) [66]. It is hypothesized that reticulation patterns surrounding hypointense SPIO enhanced liver tissue correspond to fibrotic septa surrounding regenerative nodules [67].

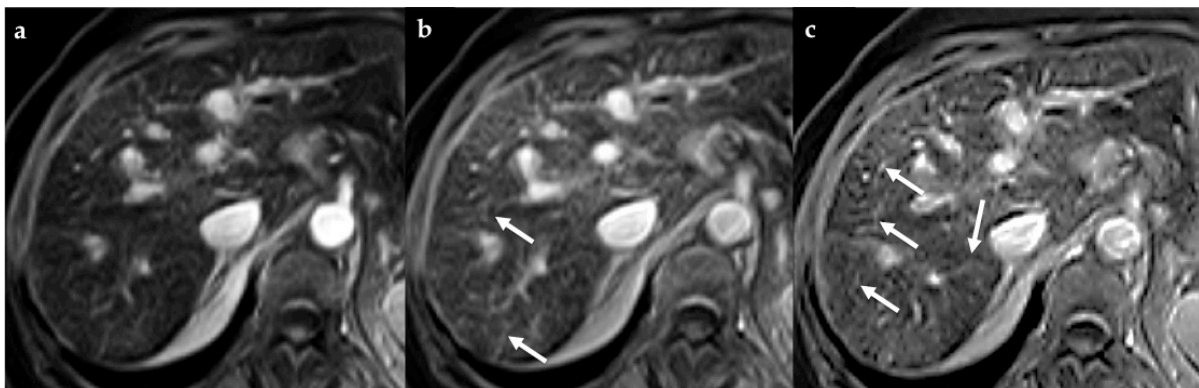


**Figure 9.** Dynamic enhancement patterns in fibrous tissue after administration of a gadolinium-based contrast agent. Axial 3D T1-weighted images obtained in the (a) arterial phase, (b) portal venous phase, and (c) 3 min after intravenous injection of a gadolinium-based contrast agent, show the progressive enhancement of the fibrotic reticulations in the liver parenchyma.

Gd-EOB-DTPA, a derivative of gadopentetate dimeglumine (Gd-DTPA), known generically as gadoxetic acid (Primovist, Bayer Schering, Berlin, Germany), is a recent hepatocyte-specific MR contrast agent and has been used to detect and characterize various hepatic tumors [68, 69]. Similar to Gd-DTPA, Gd-EOB-DTPA can be used as bolus injection. This contrast agent is actively transported from the sinusoidal space into liver cells and causes intense parenchymal enhancement, beginning within 1 or 2 min of contrast agent injection. The enhancement peaks at around 20 min and lasts for at least 2 h. Unlike Gd-DTPA, which will return into blood

vessels thereafter and is excreted entirely by kidneys, about 50% of Gd-EOB-DTPA is secreted through the biliary system, and the other 50% is secreted by kidney [70]. Deterioration of hepatic function would decrease the excretion of Gd-EOB-DTPA, because it needs adenosine triphosphate (ATP) for energy to secrete into the bile ducts by hepatocyte [71, 72]. In fact, in livers with good hepatic function, intense enhancement occurs. In livers without good function, due to cholestasis or hepatocellular dysfunction, enhancement of liver parenchyma may be weak. Using this contrast medium liver fibrosis can appear as an area of low signal intensity due to decreased hepatic function from fibrosis (Figure 11). Recent dynamic contrast-enhanced MRI studies have shown promising results using Gd-EOB-DTPA. Lee et al. [73] reported a significant alteration in signal intensity change between a group of patients with liver cirrhosis or chronic hepatitis and healthy subjects in the hepatocyte phase 20 min after contrast agent administration. In addition, Watanabe et al. [74] demonstrated that the contrast enhancement index significantly correlated with fibrosis stage. Clinical trials are currently under way to prospectively assess fibrosis staging with this contrast agent.

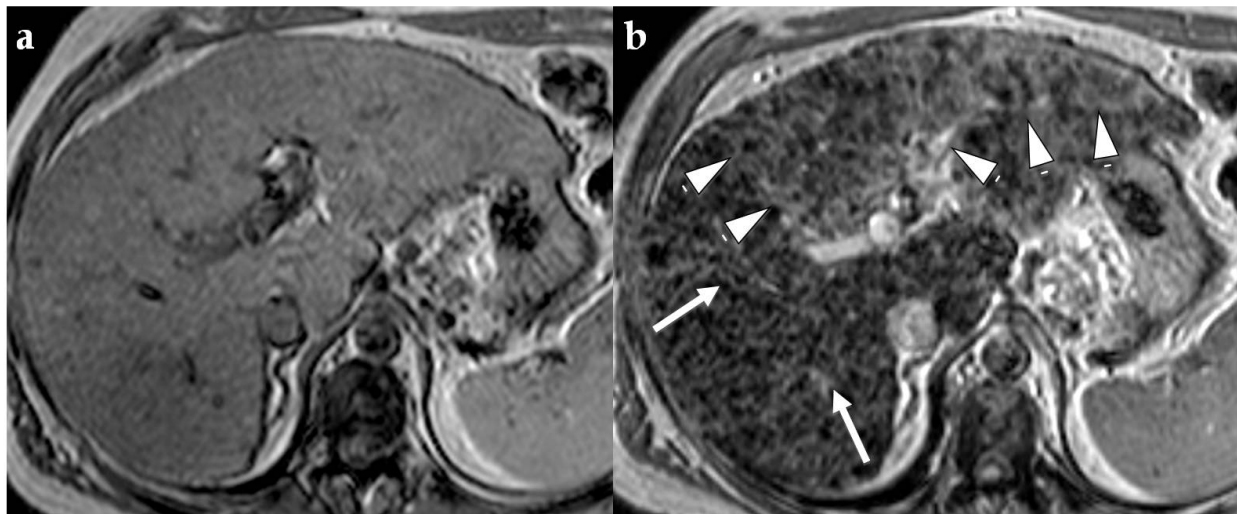


**Figure 10.** Advanced fibrosis and infiltrative HCC in a 46-year-old man with HCV-related cirrhosis. T2\*-weighted gradient-echo images obtained before (a) and after (b) intravenous SPIO injection. After injection, fibrotic reticulations in the right lobe have diminished Kupffer cell density, do not accumulate iron oxides, and hence appear relatively hyperintense (arrows in b). The left lobe is expanded and shows a wedge-shaped mass with heterogeneous hyperintensity (arrowheads in b) in the hepatocellular phase, suggestive for infiltrative HCC.

**Double-contrast enhanced MRI.** Double-contrast MRI (DC-MRI) using extracellular contrast agents in combination with SPIO particles was shown to sensitively detect liver fibrosis and depict HCC in cirrhotic livers [75]. During DC-MRI, two contrast media boli with a synergistic effect are applied: 1) SPIO particles infusion to observe the accumulation of SPIO particles by Kupffer cells of normal liver parenchyma or by Kupffer cells located in benign liver lesions, which causes signal loss on T2\*-weighted images followed by 2) Gadolinium chelates i.v. injection for analysis of delayed enhancement of hepatic septal and bridging fibrosis on T1-weighted images with fat suppression. The consequence is high image contrast between the low-signal-intensity liver parenchyma and high-signal-intensity fibrotic reticulations (Figure

12) [76]. Aguirre et al. [77] examined 101 CLD patients who underwent DC-MRI to detect hyperintense reticulations, which are postulated to represent septal fibrosis, and hypointense nodules thought to represent regenerating nodules. They achieved an accuracy of greater than 90% for the diagnosis of advanced hepatic fibrosis ( $F \geq 3$ ) compared with histopathological analysis. Recently, Fischer et al. [78] assessed the performance of semiquantitative measurement of liver perfusion from analysis of SPIO induced signal-dynamics. In this study 31 patients, including 18 patients with biopsy proven liver cirrhosis, prospectively underwent DC-MRI with dynamic T2\*-weighted gradient echo imaging after SPIO bolus injection measuring hepatic blood flow index (HBFI) and splenic blood flow index (SBFI). Significant inverse correlation was seen between HBFI and presence of liver cirrhosis resulting in a significant decrease of HBFI in patients suffering of cirrhosis compared with patients with healthy livers ( $P < 0.05$ ).

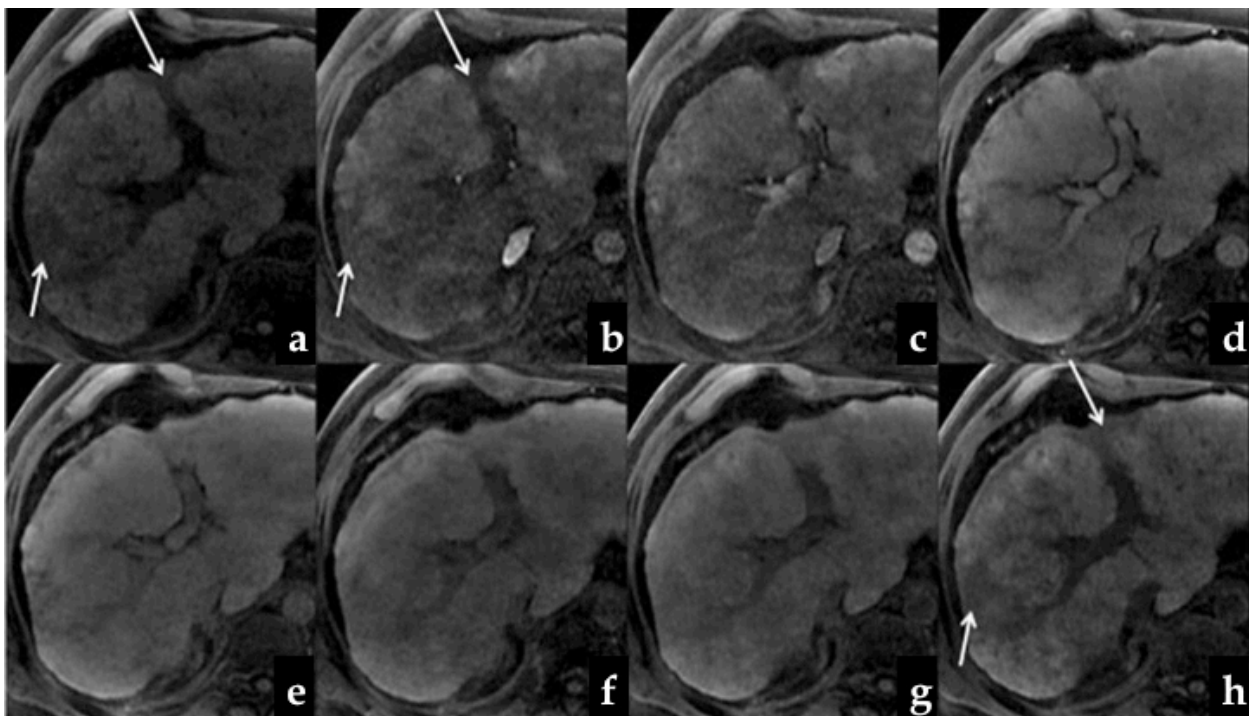


**Figure 11.** Confluent fibrosis in a 56-year-old man with cirrhosis. Precontrast (a), arterial phase (b, c), portal venous phase (d), 3 min (e), 5 min (f), 8 min (g), and hepatocellular phase (h). Wedge-shaped ill-defined areas associated with capsular retraction, with decreased enhancement in the dynamic phases and with no uptake of Gd-EOB-DTPA in the HCP (arrows).

An advantage of DC-MRI is that it works on routine imaging units and does not require specialized equipment. Computer-based texture analysis techniques may assess texture abnormalities qualitatively or quantitatively. The high cost and inconvenience associated with use of two contrast agents represent the main limitations of DC-MRI. Moreover, minor adverse events have been associated with use of SPIO, such as back pain, which has been reported in about 10% of cirrhotic patients during infusion of the particles. It is usually associated with rapid injection of SPIO and resolves after the injection is paused [79].

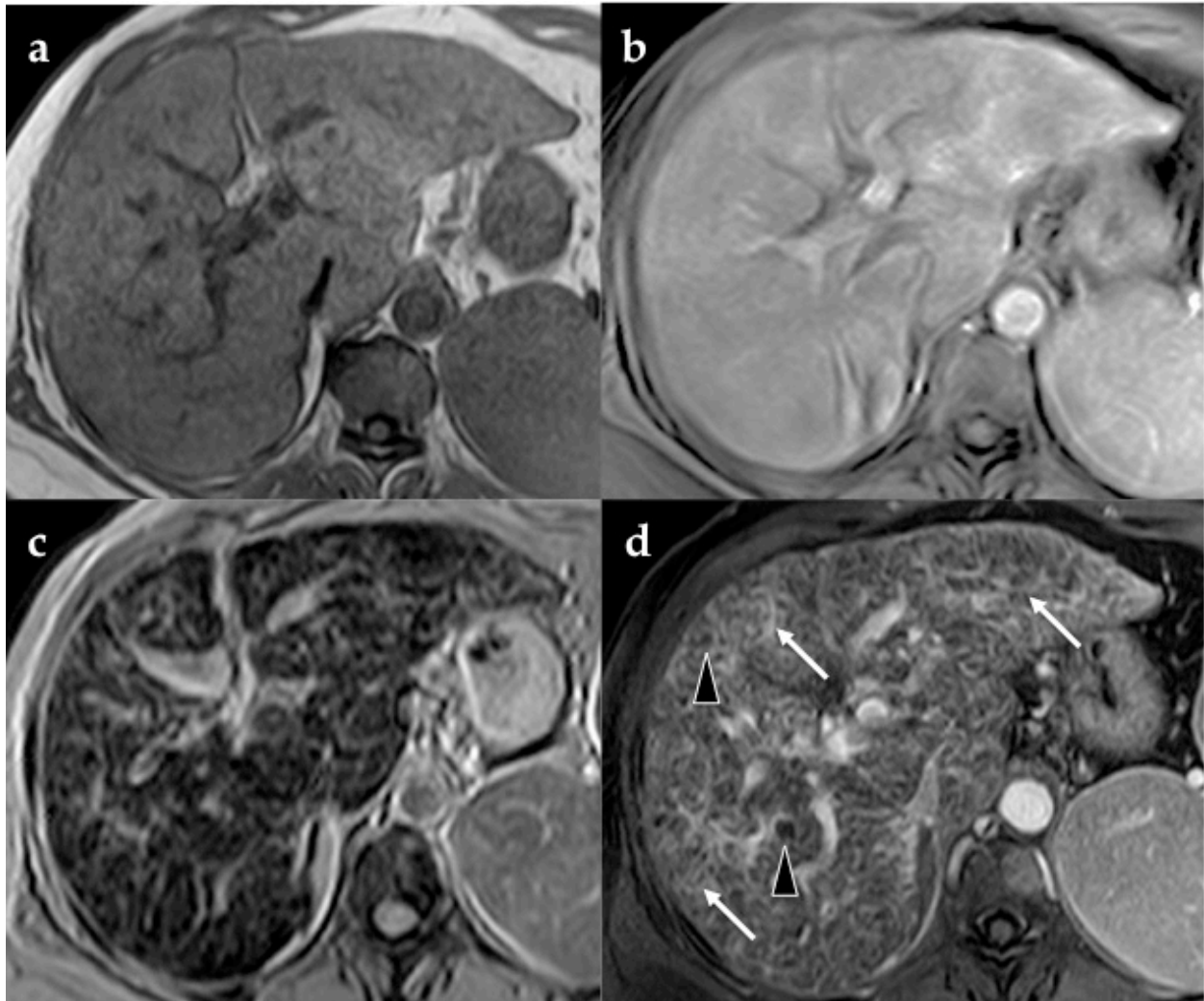


**Figure 12.** Double contrast-enhanced MR imaging appearance of cirrhosis in a 67-year-old woman with chronic HCV infection. Axial 2D T1-weighted unenhanced image (a); axial 3D T1-weighted enhanced image 30 sec after ferucarbotran injection, thus exploiting the shortening effect on T1 relaxation time; (b), T2\*-weighted gradient-echo SPIO-enhanced image after 15 min (c); and axial 3D T1-weighted double contrast-enhanced image (d). SPIO and a gadolinium-based contrast agent are synergistic with better depiction of fibrotic reticulations (arrows in d) and regenerative nodules (arrowheads in d).

**Diffusion weighted magnetic resonance imaging.** Diffusion-weighted magnetic resonance imaging (DW-MRI) is a technique that assesses the freedom of diffusion of water protons in tissues and has been extensively applied for the early detection of cerebral ischemia. Recent advances have made it feasible to apply diffusion MRI techniques for abdominal imaging [80]. In liver fibrosis, extracellular collagen fibers, glycosaminoglycans and proteoglycans may inhibit molecular diffusion of water, which suggest that DWI can be an effective method for the evaluation of fibrosis.

In DW images the observed signal intensity of tissue varies inversely with the freedom of water proton diffusion. Tissues with reduced water proton diffusion will be brighter than those with normal water proton diffusion. The sensitivity of the imaging sequence to water diffusion can be altered by changing the *b* value, or *b* factor, which is dependent in a specific mathematical way on the diffusion encoding gradient waveforms [81] and increases with the duration and amplitude of the diffusion sensitizing gradients. If two or more DW images are obtained, then it is possible to calculate the apparent diffusion coefficient (ADC) of water protons in tissues, which is determined by the slope of the log intensity versus *b* value [82, 83]. Because of the relatively short T2 relaxation time of the normal liver parenchyma (approximately 46 msec at 1.5 T and 24 msec at 3.0 T) [84], the *b* values used for clinical imaging are typically no higher than 1000 sec/mm<sup>2</sup>. Applying a small diffusion weighting of *b* less than 100–150 sec/mm<sup>2</sup> nulls the intrahepatic vascular signal, creating the so-called black-blood images, which improves detection of focal liver lesions [85, 86], while higher *b* values ( $\geq 500$  sec/mm<sup>2</sup>) give diffusion information that helps assessment of liver cirrhosis and focal liver lesion characterization [87]. The calculated ADC values can be displayed as an image and quantitative analysis can be performed by placing measuring the mean value within a region of interest, which is typically positioned in the right hepatic parenchyma to avoid major vascular structures and cardiac motion artifacts (Figure 13).

Because DW images were acquired using different *b* values and protocols and likely different patient populations, ADC values of cirrhosis are not consistent throughout the literature. Examples include ADC cutoff values of  $1.41 \times 10^{-3}$  mm<sup>2</sup>/s by Taouli et al. [88],  $0.88 \times 10^{-3}$  mm<sup>2</sup>/s by Kim et al. [89],  $1.11 \times 10^{-3}$  mm<sup>2</sup>/s by Girometti et al. [90], and more recently  $1.63 \times 10^{-3}$  mm<sup>2</sup>/s by Kovač et al. [91]. Although there are various ADC values for the diagnosis of cirrhosis, the cirrhotic liver tissues consistently have significantly lower ADC values compared with liver tissues with no fibrosis as seen in prior studies [92–94]. Previously published studies with DWI showed moderate sensitivity and specificity in distinguishing advanced fibrosis to cirrhosis (F3–F4) from lesser degrees of fibrosis. However, considerable overlap in ADC values between tissues with cirrhosis and with no to moderate fibrosis was also observed.

In a recent study, Bakan et al. [95] performed DWI with *b*-factors of 0, 500 and 1000 s/mm<sup>2</sup> in order to investigate the relationship between ADC values and liver inflammation (HAI scores). They found that as HAI scores increased there was a statistically significant decrease in ADC values ( $P < 0.01$ ). However, differences in MRI equipment and sequence parameters make it difficult to compare studies. In addition, despite technical improvements in DWI, the method remains sensitive to susceptibility and motion-related artifacts, and it is difficult to obtain images with sufficient quality for reliable quantitative analysis on a consistent basis. Further studies are required to create a standard setup for DWI to make studies comparable and to evaluate how various ADC values of liver tissue other than fibrosis may be influenced by other factors associated with chronic liver diseases.

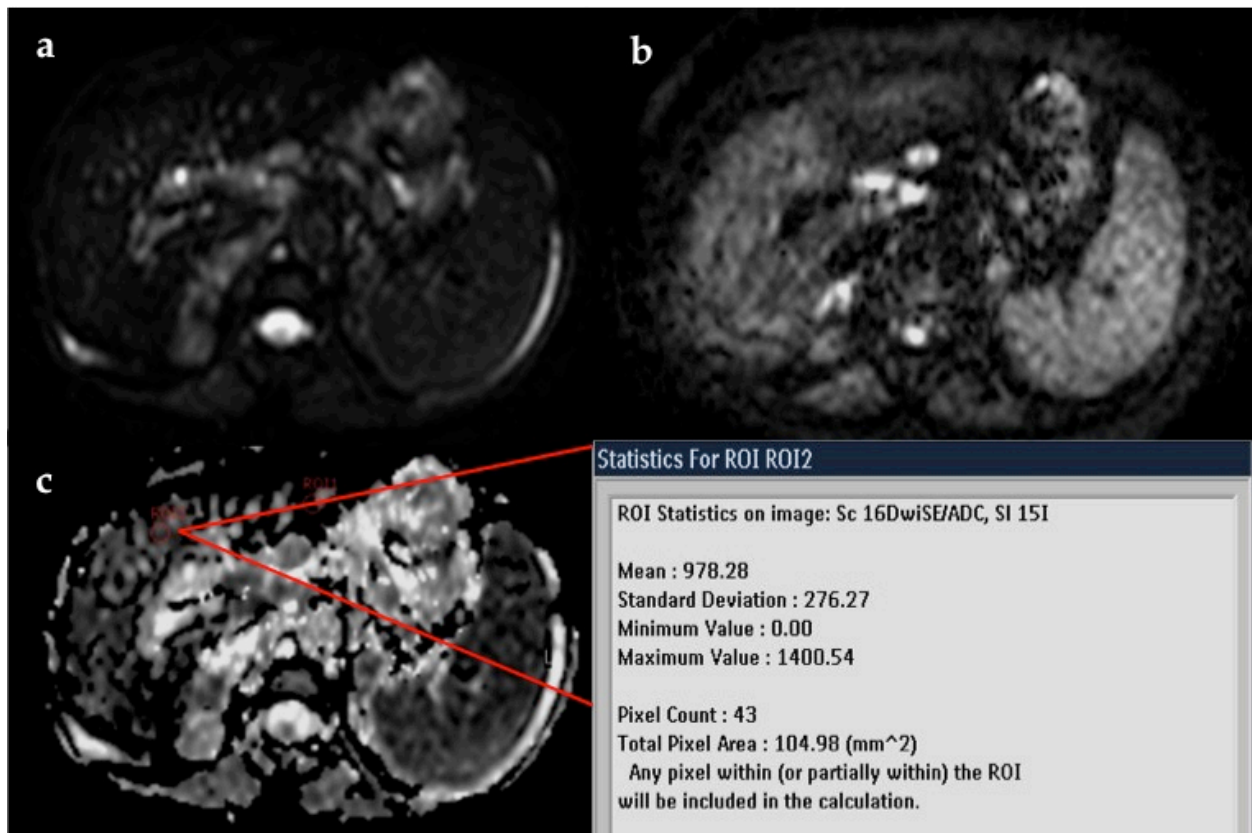


**Figure 13.** year-old man with biopsy-proven hepatitis C and related stage III fibrosis. Diffusion-weighted images obtained with b value of 0 (a) and 800 (b) s/mm<sup>2</sup> and apparent diffusion coefficient (ADC) map (c) are shown. Mean ADC value was  $0.98 \times 10^{-3}$  mm<sup>2</sup>/s.

**MR Elastography.** A new option for assessing shear stiffness in various tissue types, including liver fibrosis, is MR Elastography (MRE) [96]. MRE uses a modified phase contrast technique to sensitively image the propagation characteristics of acoustic shear waves that are generated with the organ of interest [97]. This system consisted of an acoustic driver system, a gradient-echo MRE pulse sequence, and special software for data analysis. A 19cm diameter, 1.5cm thick cylindrical passive driver is placed against the right chest wall over the liver with the center of the driver at the level of the xiphoid of the sternum (Figure 14). The passive driver is held in place with an abdominal binder. Continuous acoustic vibration at frequencies between 40 and 120 Hz transmits from an active driver to the passive driver through a flexible vinyl tube was used to produce propagating shear waves in the liver [98-100]. When the pneumatic device is activated, the patient will feel vibrations in the rib cage due to the pressure waves. MR images are acquired with a gradient-echo sequence as the waves propagate through the liver. The velocity and wavelength of the waves propagating in the abdomen depend on the stiffness of the tissue (velocity and wavelength increase with greater tissue stiffness), enabling the stiffness estimation [101].

A specialized phase-contrast MRI sequence is then used to image the propagating waves in the liver. This sequence uses motion-encoding gradients that are oscillated synchronously with the applied vibrations, allowing waves with amplitudes in the micron range to be readily

imaged. Each MRE acquisition provides an image that represents the displacement caused by shear wave propagation in the medium. The wave images are then processed using a specially developed inversion algorithm to generate quantitative images called elastograms [96]. Elastograms are maps of tissue stiffness shown on a color scale ranging from soft to hard. Mean elasticity values measured in regions of interest within the liver are obtained. The unit of measurement for elasticity is kilopascal (kPa), as it is with ultrasound-based transient elastography (TE) (Figure 15). Each MRE examination is performed during a single breath-hold of 10 to 30 seconds to allow imaging of wave propagation, in addition to the standard 30-40 minute MRI examination of the abdomen [102].

Initial studies in patients with a spectrum of liver disease types have shown that liver stiffness as measured with MRE increases as the stage of fibrosis advances. The differences in stiffness between patients with early stages of fibrosis (F0 vs F1 vs F2) are small and there is overlap between groups, but the differences between groups with higher stages (F2 vs F3 vs F4) are large, with little overlap between groups [99, 102].

As for ADC values in DWI examinations, a variety of MRE cutoff values are observed throughout the literature. In a recent study, to identify fibrosis stage  $\geq 2$  (F2–F4) and stage  $\geq 3$  (F3–F4), Wang et al. [103] reported sensitivity of 91% and 92% and specificity of 97% and 95% with cutoff values of 5.37 and 5.97 kPa, respectively. Huwart et al. [104] showed similar high sensitivity of 98% and 95% and specificity of 100% and 100% for discrimination, although relatively lower cutoff values of 2.5 kPa and 3.1 kPa were used. The variability of cutoff values observed may be potentially explained by MRE different scanner manufacturers, case mixes, imaging protocols, and post-processing procedures.

As reported by Rustogi et al. [105] stiffness measurements are repeatable with high overall inter-reader agreement ( $P=0.74$ ); thus, MRE shows potential for longitudinal monitoring of patients. Furthermore, Yin et al. found that this technique has a high negative predictive value (97%) for excluding the presence of fibrosis, suggesting that MRE could have a role for improving the ability to risk-stratify patients for liver biopsy [102].

MRE benefits from the intrinsic advantages of MR imaging, such as freely oriented field of view, no “acoustical window” requirement, the ability to quantify steatosis, operator independence, and the ability to perform conventional liver MRI at the same time. In addition, MRE is relatively unaffected by the patient’s body habitus and the presence of ascites, as shear waves generated in vivo in MRE have good hepatic penetration.

Nevertheless MRE has some limitations. The most important one is that MRE measures a surrogate of liver fibrosis (tissue stiffness) rather than fibrosis itself. A variety of factors may confound MRE assessment of liver fibrosis, including hepatic inflammation, steatosis, hepatic vascular congestion, cholestasis, and portal hypertension. Moreover, the selection of significant regions of interest is subjective and requires judgment and experience. As with the other techniques, efforts to standardize the equipment and techniques used for MRE should be practiced to maximize diagnostic accuracy and enable comparison of results in different settings. Further prospective evaluation is required for characterizing the diagnostic performance of MRE.

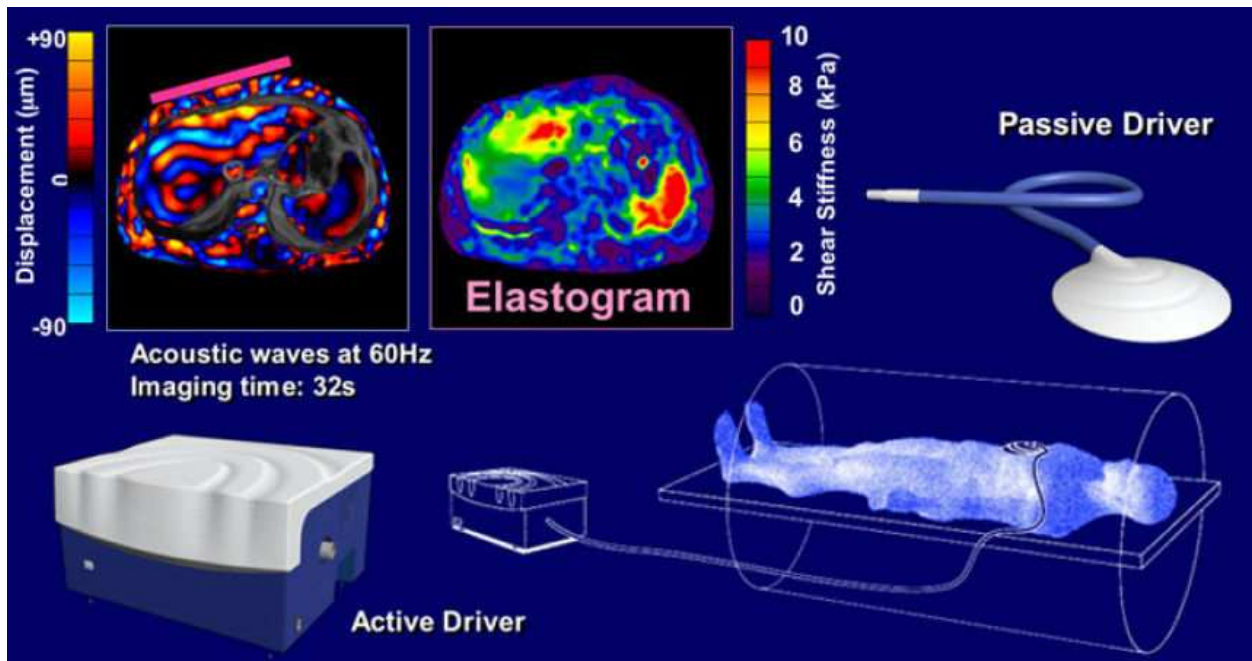


**Figure 14.** A remote acoustic driver pumps air into a pneumatic device strapped onto the patient's body, eliciting tissue displacement, which is measured by MRE and used to derive images showing tissue stiffness.

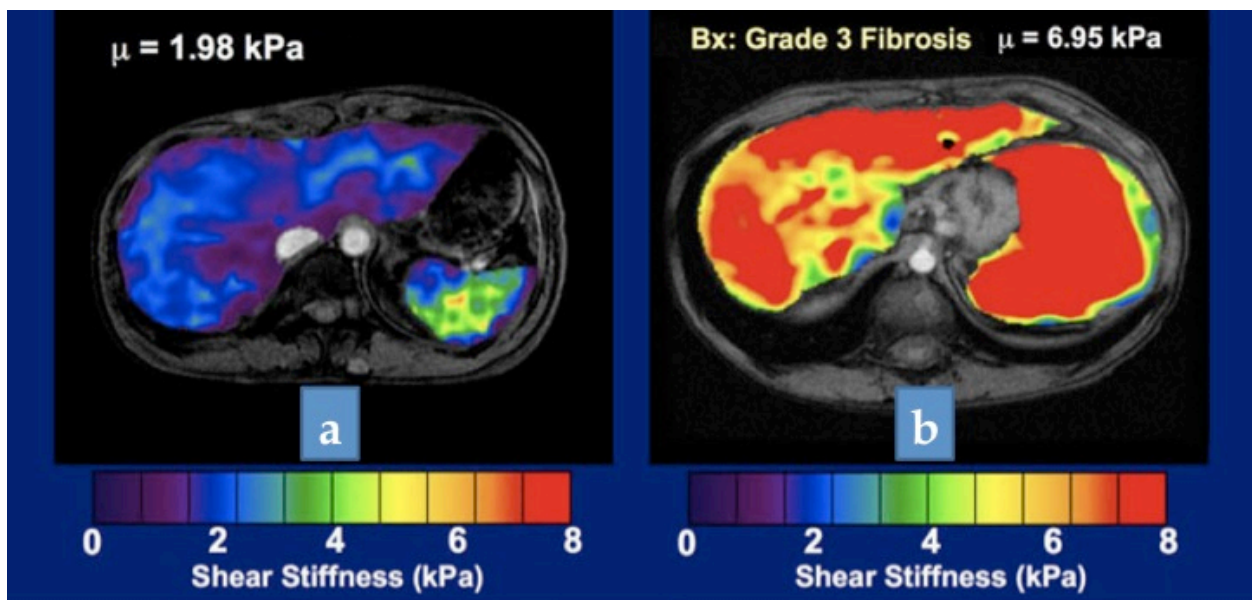


**Figure 15.** An elastogram of a healthy liver (a) showing a post processed value of 1.98 kPa corresponding to normal tissue stiffness. An elastogram of the liver of a patient with Grade 3 fibrosis (b), with a shear stiffness value of 6.95 kPa.

**Perfusion MRI.** Perfusion MRI provides a method of measuring perfusion changes in the liver. Liver fibrosis gradually led to a loss of normal fenestrae, due to deposition of basement membrane and new formation of capillary tight junctions along the sinusoids (phenomenon of capillarization). There is also deposition of fibers by activated hepatic stellate cells, which results in enlargement of the Space of Disse. Consequently, intrahepatic vessels and sinusoids

obliteration reduces passage of blood through the parenchyma, producing increase in hepatic arterial perfusion and decrease in portal venous perfusion. Several studies have shown that careful kinetic modeling of dynamic contrast-enhanced (DCE) MR images can noninvasively quantify regional and global changes in hepatic perfusion associated with liver cirrhosis and fibrosis [106-109].

For perfusion MRI of the liver, a rapid injection of a low-molecular-weight gadolinium-chelate contrast is necessary, using a programmable pump injector. It is recommended the intravenous administration of Gd-DTPA (0.1-0.2 mmol of contrast medium/kg body weight) followed by a 20ml saline flush, at an injection rate of 3–5 ml/s. T1-weighted 3D spoiled gradient echo sequence is typically performed, with whole liver coverage and high temporal resolution (i.e. repeated imaging of the same area in the liver about every 4 s). An oblique imaging plane (oblique coronal) is particularly useful in order to include the aorta and the portal vein in the same image sections. Patients are generally instructed to fast for 4–6 h prior to the scan, given the potential changes in portal venous flow occurring in the post-prandial state.

The analysis can be performed by semi-quantitative or quantitative techniques. One semi-quantitative description of liver vascularity is the hepatic perfusion index (HPI), which describes the relative contribution of arterial vs portovenous flow to the total liver perfusion. The HPI has been investigated using different imaging techniques, and appears to provide biologically meaningful information despite its relative simplicity [110]. For quantitative methods, regions of interest (ROIs) are placed over the area of interest to generate signal intensity (SI) versus time curve. Typically, arterial input function is obtained by placing a ROI on the abdominal aorta. Portal input function is obtained from a ROI placed on the main portal trunk, and a ROI at the level of hepatic parenchyma to measure the time–activity curve. Several kinetic models are currently in use for the assessment of liver perfusion. Single-input models assume that the vascular input is derived from the hepatic artery only, whereas dual-input models assume that the vascular input is derived from both the hepatic artery and the portal vein. Single compartment models assume that the contrast is confined to only one compartment (i.e. vascular space), whereas dual compartment models assume that there is dynamic distribution of contrast between two compartments (i.e. the vascular space and the interstitial space). Therefore, numerous perfusion parameters can be estimated, including absolute portal venous blood flow, absolute arterial blood flow, absolute total liver blood flow, portal venous fraction, arterial fraction, distribution volume (DV), and mean transit time (MTT) [111].

In a previous study, Annet et al. [106] have investigated a dual-input single compartment model and have demonstrated altered arterial, portal and total liver perfusion, as well as increased MTT in cirrhotic livers compared to non-cirrhotic livers, and found a correlation with severity of disease as assessed by the Child-Pugh class and degree of portal hypertension. In a recent study, Leporq et al. [112] applied dual-input single-compartment model and quantitative perfusion parameters for the noninvasive assessment of liver fibrosis. HPI, arterial and portal perfusion, tissue blood volume, and MTT showed a significant difference between nonadvanced fibrosis (F0–F2) and advanced fibrosis (F3–F4). In addition, HPI and portal perfusion showed a strong correlation with the fibrosis score ( $P < 0.001$ ). Chen et al. performed a prospective study using Gd-EOB-DTPA in patients with chronic hepatitis to calculate

perfusion parameters by applying a dual-input single compartment model. They found a significant increase in arterial perfusion at 60 s and 100 s in patients compared with healthy subjects and a significant difference in arterial perfusion when three different fibrotic subgroups (none, mild and advanced) were compared at 60 s [113].

Several factors limit the correlation between perfusion parameters and fibrosis, such as cardiac status, fasting state, hepatic congestion, hepatic inflammation, hepatic lesions, and portal venous flow. Other limitations include differences in technical parameters, imaging system, and use of different pharmacokinetic models [114]. In addition, relevant is the laborious post-processing required to obtain quantitative perfusion parameters. However, standardization of imaging acquisition and analysis techniques need to be actively addressed for the technique to be widely adopted.

**MR Spectroscopy.** MR spectroscopy (MRS) enables the non-invasive measurement of concentrations of different chemical components within tissues, which are displayed as a spectrum with peaks consistent with the various chemicals detected. The liver is considered an ideal organ for MRS investigation due to its anatomical location and increased metabolic demands [115, 116]. MRS of the liver is performed using a whole body MRI system at field strengths of 1.5 Tesla (T) or higher. The patient lies supine on the MRI table with RF coils positioned appropriately. After a standard MR imaging for localization, special MR pulse sequences are applied to generate spectroscopic data within the appropriate anatomical location and volume (defined by voxels) of interest. A typical examination will take 45 to 60 minutes. The spectral analysis of data requires processing to reduce noise and perform analysis. Metabolite concentrations can be expressed in absolute or relative terms. In general, the peak area of a metabolite signal is directly related to its concentration. Whereas a number of *in vivo* studies have explored the diagnostic performance of MRS for characterizing hepatic lesions [117], more recently there has been some interest in the role of MRS for detecting hepatic fibrosis. MRS is most commonly used to assess signals from hydrogen ( $^1\text{H}$ ) and phosphorus ( $^{31}\text{P}$ ).

$^1\text{H}$ -based MRS is widely used for the quantification of hepatic lipid. *In vitro* MRS studies of oils [118] and intact liver tissue [119] have demonstrated that lipid resonances might be quantified to derive indices of lipid composition, including saturation and polyunsaturation. These compositional indices differed between obese patients with and without hepatic steatosis. Indices of lipid composition using *in vivo* proton ( $^1\text{H}$ ) MRS at 1.5 Tesla have been shown to delineate the severity of fibrosis in patients with chronic hepatitis C (in whom hepatic steatosis is prevalent) [120]. In patients with chronic HCV infection, as fibrosis advances, steatosis tends to recede [121]. McPherson et al. [122] confirmed this inverse relation and found that with  $^1\text{H}$ -MRS, the percentage of steatotic hepatocytes in patients with more advanced fibrosis tended to be underestimated. However, because  $^1\text{H}$ -MRS yields an estimate of proton density fat fraction and not a measure of the degree of hepatocellular involvement, this result would be expected. When ROCs were generated for the diagnosis of steatosis with  $^1\text{H}$ -MRS according to fibrosis stage, the values were only slightly lower in cases of more advanced fibrosis (AUC, 0.97 for F=0–1 vs 0.95 for F=2–3). More recently, Georgoff et al. [123] also found only a small decrease in the ROC for  $^1\text{H}$ -MRS in subjects with fibrosis (AUC, 0.96 for F=0 vs 0.92 for F=1–4).

<sup>31</sup>P-based MRS has also shown promise as a method of assessing the degree of hepatic fibrosis, in particular through analysis of the phosphomonoester/phosphodiester (PME/PDE) ratio [124]. As the stage of fibrosis increases, the PME peak may represent extensive membrane remodeling due to elevated levels of cell membrane precursors (such as phosphocholine and phosphoethanolamine). At the same time, there is a reduction in the PDE peak owing to reduced levels of membrane degradation products such as glycerophosphorylethanolamine and glycerylphosphorylcholine. Therefore, changes in the PME/PDE ratio are thought to reflect an increase in the regenerative efforts made by the damaged liver [125]. Moreover, <sup>31</sup>P-MRS had a sensitivity and specificity of 82% and 81% respectively for cirrhosis and showed statistically significant differences between mild hepatitis, moderate hepatitis, and cirrhosis [126].

Several limitations with current MRS approaches, however, are observed. The major problem in obtaining MRS signals from abdominal organs is sensitivity to physiologic movement during the scan time usually exceeding several minutes. Various methods of reducing movement, such as breath holding and placing patients in the prone position during signal acquisition, have been used [127]. Furthermore MRS requires considerable operator skills (sequence programming, shimming, analysis of spectra) and access to special equipment. Most studies contain small numbers of patients from heterogeneous populations assessed by varying MRS methods. In addition, the variation in reproducibility of data acquisition from healthy volunteers can range between 4% and 20% for both subject and examination. Ultimately, the role of *in vivo* MRS for detecting hepatic fibrosis requires assessment in larger diagnostic accuracy studies among patients with various hepatobiliary disorders.

## 5. Conclusion and future directions

A fast, safe and reliable technique to assess fibrosis of CLD and to follow up progression or regression of fibrosis during treatment is required. Ultrasound is still a widespread, low cost, user-friendly, and accurate technique. However, it may not have a high specificity due to limitations related to the patient or operator and its role is probably more oriented to patient's selection and follow-up. MRI is a more "challenging" method for radiologists and especially for patients, with limitations related to: the availability of high performance scanner; the presence of experienced personnel; the examination's timing and to its less tolerability. MRI may, however, represent the one-stop shop technique, allowing the diagnosis and characterization of fibrosis but also the overall assessment of CLD. In addition, MRI is more research-oriented, since its multiparametric potential, allows not only distinguishing the various fibrosteatotic alterations but also performing metabolic assessments. This last feature permits studies on the pathogenetic mechanisms and on drug therapies studies.

The diagnostic performances of all described noninvasive radiologic modalities were better in distinguishing patients with cirrhosis from lesser degrees of fibrosis. However, staging of fibrosis was rarely achieved reliably. In conclusion, to date, the most promising techniques appear to be Transient Elastography [59] and MRE [128, 129] since they provide reliable results in detecting severe fibrosis and future developments promise to increase the reliability and

accuracy of staging of hepatic fibrosis. In the future, MRI technical development and new contrast agents could permit imaging of fibrogenesis.

## Author details

Luca Macarini and Luca P. Stoppino

Department of Surgical Sciences, Section of Diagnostic Imaging, Foggia University School of Medicine, Azienda Ospedaliero-universitaria "Ospedali Riuniti", Foggia, Italy

## References

- [1] Friedman SL. Hepatic fibrosis: overview. *Toxicology* 2008;254(3):120-129.
- [2] Popper H, Uenfriend S. Hepatic fibrosis. Correlation of biochemical and morphologic investigations. *Am J Med* 1970;49:707-721.
- [3] Schaffner F, Klion FM. Chronic hepatitis. *Annu Rev Med* 1968;19:25-38.
- [4] Soyer MT, Ceballos R, Aldrete JS. Reversibility of severe hepatic damage caused by jejunoileal bypass after re-establishment of normal intestinal continuity. *Surgery* 1976;79:601-604.
- [5] Pinzani M. Liver fibrosis. *Springer Semin Immunopathol* 1999;21:475-490.
- [6] Afdhal NH, Nunes D. Evaluation of liver fibrosis: a concise review. *Am J Gastroenterol* 2004;99:1160-1174.
- [7] Thampanitchawong P, Piratvisuth T. Liver biopsy: complications and risk factors. *World J Gastroenterol* 1999;5:301-304.
- [8] Regev A, Berho M, Jeffers LJ, et al. Sampling error and intra-observer variation in liver biopsy in patients with chronic HCV infection. *Am J Gastroenterol* 2002;97:2614-2618.
- [9] Leon DA, McCambridge J. Liver cirrhosis mortality rates in Britain, 1950 to 2002. *Lancet* 2006;367(9511):645.
- [10] Leon DA, Saburova L, Tomkins S, et al. Hazardous alcohol drinking and premature mortality in Russia: a population based case-control study *Lancet* 2007;369(9578):2001-2009.
- [11] World Health Organisation. Hepatitis C. WHO Fact Sheet 2000;164:1-4.
- [12] Shepard CW, Finelli L, Alter MJ. Global epidemiology of hepatitis C virus infection. *Lancet Infect Dis* 2005;5:558-567.

- [13] Farrell GC LC. Nonalcoholic fatty liver disease: from steatosis to cirrhosis. *Hepatology* 2006;43:S99-S112.
- [14] Day CP. Natural History of NAFLD: Remarkably benign in the absence of cirrhosis. *Gastroenterology* 2005;129:375-377.
- [15] Powell EE, Edwards-Smith CJ, Hay JL, et al. Host genetic factors influence disease progression in chronic hepatitis C. *Hepatology* 2000;31:828-833.
- [16] Monto A, Patel K, Bostrom A, et al. Risks of a range of alcohol intake on hepatitis C-related fibrosis. *Hepatology* 2004;39:826-834.
- [17] Schiano TD, Kim-Schluger L, Gondolesi G, Miller CM. Adult living donor liver transplantation: the hepatologist's perspective. *Hepatology* 2001;33:3-9.
- [18] Benhamou Y, Di Martino V, Bochet M, et al. Factors affecting liver fibrosis in human immunodeficiency virus- and hepatitis C virus-coinfected patients: impact of protease inhibitor therapy. *Hepatology* 2001;34:283-287.
- [19] Farci P, Roskams T, Chessa L, et al. Long-term benefit of interferon alpha therapy of chronic hepatitis D: regression of advanced hepatic fibrosis. *Gastroenterology* 2004;126:1740-1749.
- [20] Knodell RG, Ishak KG, Black WC, et al. Formulation and application of a numeral scoring system for assessing histological activity in asymptomatic chronic active hepatitis. *Hepatology* 1981;1:431-435.
- [21] Ishak K, Baptista A, Bianchi L, et al. Histologic grading and staging of chronic hepatitis. *J Hepatol* 1995; 22:696-699.
- [22] Bedossa P, Poynard T. The METAVIR cooperative study group. An algorithm for the grading of activity in chronic hepatitis C. *Hepatology* 1996;24:289-293.
- [23] Thiese ND, Bodenheimer HC, Ferrell LD. Acute and chronic viral hepatitis. In: Burt AD, Portmann BC, Ferrell LD, eds. *MacSween's pathology of the liver*. 5th ed. Edinburgh, Scotland: Churchill Livingstone, 2006; chap 8.
- [24] Ratziu V, Charlotte F, Heurtier A, et al. Sampling variability of liver biopsy in nonalcoholic fatty liver disease. *Gastroenterology* 2005;128:1898-1906.
- [25] Bravo AA, Sheth SG, Chopra S. Liver biopsy. *N Engl J Med* 2001;344:495-500.
- [26] Piccinino F, Sagnelli E, Pasquale G, Giusti G. Complications following percutaneous liver biopsy: a multicentre retrospective study on 68,276 biopsies. *J Hepatol* 1986;2:165-173.
- [27] Colli A, Fraquelli M, Andreoletti M, et al. Severe liver fibrosis or cirrhosis: accuracy of US for detection—analysis of 300 cases. *Radiology* 2003;227:89-94.
- [28] Cohen EI, Wilck EJ, Shapiro RS. Hepatic imaging in the 21st century. *Semin Liver Dis* 2006;26:363-372.

- [29] Fritz GA, Schoellnast H, Deutschmann HA, et al. Density histogram analysis of un-enhanced hepatic computed tomography in patients with diffuse liver diseases. *J Comput Assist Tomogr* 2006;30:201-205.
- [30] Colagrande S, Centi N, Galdiero R, Ragozzino A. Transient hepatic intensity differences: part 2, those not associated with focal lesions. *AJR Am J Roentgenol* 2007;188:160-166.
- [31] Partanen KP. Dynamic CT of liver cirrhosis. *Invest Radiol* 1984;19:303-308.
- [32] Ito K, Mitchell DG, Gabata T, Hussain SM. Expanded gallbladder fossa: simple MR imaging sign of cirrhosis. *Radiology* 1999;211:723-726.
- [33] Hussain SM, Semelka RC. Hepatic imaging: comparison of modalities. *Radiol Clin North Am* 2005;43:929-947.
- [34] Roulot D, Czernichow S, Le Clesiau H, et al. Liver stiffness values in apparently healthy subjects: Influence of gender and metabolic syndrome. *J Hepatol* 2008;48:606-613.
- [35] Fraquelli M, Rigamonti C, Casazza G, et al. Reproducibility of transient elastography in the evaluation of liver fibrosis in patients with chronic liver disease. *Gut* 2007;56:968-973.
- [36] Sandrin L, Fourquet B, Hasquenoph JM, et al. Transient elastography: A new non-invasive method for assessment of hepatic fibrosis. *Ultrasound Med Biol* 2003;29:1705-1713.
- [37] Konate A, Boursier J, Reaud S, et al. Liver stiffness measurement by transient elastography: predictive factors of accuracy, success and reproducibility. *J Hepatol* 2006;44:S195.
- [38] Ziol M, Handra-Luca A, Kettaneh A, et al. Non-invasive assessment of liver fibrosis by measurement of stiffness in patients with chronic hepatitis C. *Hepatology* 2005;41:48-54.
- [39] Carrion JA, Navasa M, Bosch J, et al. Transient elastography for diagnosis of advanced fibrosis and portal hypertension in patients with hepatitis C recurrence after liver transplantation. *Liver Transpl* 2006;12:1791-1798.
- [40] Foucher J, Chanteloup E, Vergniol J, et al. Diagnosis of cirrhosis by transient elastography (FibroScan): a prospective study. *Gut* 2006;55:403-408.
- [41] Nguyen-Khac E. Results and place of fibroscan in the noninvasive diagnosis of hepatic fibrosis. *Rev Med Interne* 2007;28:94-102.
- [42] Castera L, Vergniol J, Foucher J, et al. Prospective comparison of transient elastography, Fibrotest, APRI, and liver biopsy for the assessment of fibrosis in chronic hepatitis C. *Gastroenterology* 2005;12:343-350.

- [43] Marcellin P, Ziol M, Bedossa P, et al. Non-invasive assessment of liver fibrosis by stiffness measurement in patients with chronic hepatitis B. *Liver Int* 2009;29:242-247.
- [44] de Ledinghen V, Douvin C, Kettaneh A, et al. Diagnosis of hepatic fibrosis and cirrhosis by transient elastography in HIV/hepatitis C viruscoinfectd patients. *J Acquir Immune Defic Syndr* 2006;41:175-179.
- [45] Yoneda M, Yoneda M, Mawatari H, et al. Noninvasive assessment of liver fibrosis by measurement of stiffness in patients with nonalcoholic fatty liver disease (NAFLD). *Dig Liver Dis* 2008;40:371-378.
- [46] Corpechot C, El Naggar A, Pujol-Robert A, et al. Assessment of biliary fibrosis by transient elastography in patients with PBC and PSC. *Hepatology* 2006;43:1118-1124.
- [47] Ophir J, Cespedes I, Ponnekanti H, Yazdi Y, Li X. Elastography: a quantitative method for imaging the elasticity of biological tissues. *Ultrason Imaging* 1991;13:111-134.
- [48] Pesavento A, Krueger C, Ermert H. A time efficient and accurate strain estimation concept for ultrasonic elastography using interactive phase zero estimation. *IEEE Trans an Ultrason Ferroelect Freq Contr* 1999;46:1057-1067.
- [49] Frey H. Realtime elastography. A new ultrasound procedure for the reconstruction of tissue elasticity *Radiologe* 2003; 43:850-855.
- [50] Itoh A, Ueno E, Tohno E, Kamma H, Takahashi H, Shiina T, Yamakawa M, Matsu-mura T. Breast disease: clinical application of US elastography for diagnosis. *Radiology* 2006; 239:341-350.
- [51] Srinivasan S, Kallel F, Ophir J. The effects of digitization on the elastographic signal-to-noise ratio. *Ultrasound Med Biol* 2002; 28:1521-1534.
- [52] Friedrich-Rust M, Ong MF, Herrmann E et al. Real-time elastography for noninvasive assessment of liver fibrosis in chronic viral hepatitis. *AJR Am J Roentgenol* 2007;188:758-764.
- [53] Wang J, Guo L, Shi X, et al. Real-time elastography with a novel quantitative technology for assessment of liver fibrosis in chronic hepatitis B. *Eur J Radiol* 2012;81:e31-e36.
- [54] Zhai L, Palmeri ML, Bouchard RR, et al. An integrated indenter-ARFI imaging system for tissue stiffness quantification. *Ultrason Imaging* 2008;30:95-111.
- [55] Nightingale K, Soo MS, Nightingale R, Trahey G. Acoustic radiation force impulse imaging: in vivo demonstration of clinical feasibility. *Ultrasound Med Biol* 2002;28:227-235.
- [56] Mauldin FW Jr, Zhu HT, Behler RH, et al. Robust principal component analysis and clustering methods for automated classification of tissue response to ARFI excitation. *Ultrasound Med Biol* 2008;34: 309-325.

- [57] Sporea I, Badea R, Sirli R, et al. How efficient is acoustic radiation force impulse elastography for the evaluation of liver stiffness? *Hepat Mon.* 2011;11:532-538.
- [58] Friedrich-Rust M, Nierhoff J, Lupsor M, et al. Performance of Acoustic Radiation Force Impulse imaging for the staging of liver fibrosis: a pooled meta-analysis. *J Viral Hepat* 2012;19:e212-219.
- [59] Colombo S, Buonocore M, Del Poggio A, et al. Head-to-head comparison of transient elastography (TE), real-time tissue elastography (RTE), and acoustic radiation force impulse (ARFI) imaging in the diagnosis of liver fibrosis. *J Gastroenterol* 2012;47:461-469.
- [60] Martin DR. Magnetic resonance imaging of diffuse liver diseases. *Top Magn Reson Imaging* 2002;13:151-163.
- [61] Ito K, Mitchell DG, Siegelman ES. Cirrhosis: MR imaging features. *Magn Reson Imaging Clin N Am* 2002;10:75-92.
- [62] Dodd GDI, Baron RL, Oliver JHI, Federle MP: Spectrum of imaging findings of the liver in end-stage cirrhosis: Part I. Gross morphology and diffuse abnormalities. *AJR Am J Roentgenol* 1999;173:1031-1036.
- [63] Brancatelli G, Federle MP, Ambrosini R, et al. Cirrhosis: CT and MR imaging evaluation. *Eur J Radiol* 2007;61:57-69.
- [64] Balci NC, Semelka RC. Contrast agents for MR imaging of the liver. *Radiol Clin North Am* 2005;43:887-898.
- [65] Hundt W, Petsch R, Helmberger T, Reiser M. Signal changes in liver and spleen after Endorem administration in patients with and without liver cirrhosis. *Eur Radiol* 2000;10:409.
- [66] Lucidarme O, Baleston F, Cadi M, et al. Non-invasive detection of liver fibrosis: is superparamagnetic iron oxide particle-enhanced MR imaging a contributive technique? *Eur Radiol* 2003;13:467-474.
- [67] Elizondo G, Weissleder R, Stark DD, et al. Hepatic cirrhosis and hepatitis: MR imaging enhanced with superparamagnetic iron oxide. *Radiology* 1990;174:797-801.
- [68] Ahn SS, Kim MJ, Lim JS, et al. Added value of gadoxetic acid-enhanced hepatobiliary phase MR imaging in the diagnosis of hepatocellular carcinoma. *Radiology* 2010;255:459-466.
- [69] Ichikawa T, Saito K, Yoshioka N, et al. Detection and characterization of focal liver lesions: a Japanese phase III, multicenter comparison between gadoxetic acid disodium-enhanced magnetic resonance imaging and contrast-enhanced computed tomography predominantly in patients with hepatocellular carcinoma and chronic liver disease. *Invest Radiol* 2010;45:133-141.

- [70] Reimer P, Rummeny EJ, Shamsi K, et al. Phase II clinical evaluation of Gd-EOB-DTPA: dose, safety aspects, and pulse sequence. *Radiology* 1996;199:177-183.
- [71] Tsuda N, Matsui O. Cirrhotic rat liver: reference to transporter activity and morphologic changes in bile canaliculi— gadoxetic acid-enhanced MR imaging. *Radiology* 2010;256:767-773.
- [72] Nilsson H, Nordell A, Vargas R, et al. Assessment of hepatic extraction fraction and input relative blood flow using dynamic hepatocyte-specific contrast-enhanced MRI. *J Magn Reson Imaging* 2009;29:1323-1331.
- [73] Lee WJ, Cha SH, Kim MY, et al. Quantitative evaluation of the hepatic parenchymal change in patients with chronic liver disease using Gd-EOB-DTPA-enhanced MRI: comparison with normal liver. *J Korean Soc Radiol* 2011;64:49-55.
- [74] Watanabe H, Kanematsu M, Goshima S, et al. Staging hepatic fibrosis: comparison of gadoxetate disodium-enhanced and diffusion-weighted MR imaging—preliminary observations. *Radiology* 2011;259:142-150.
- [75] Macarini L, Marini S, Milillo P, et al. Double-contrast MRI (DC-MRI) in the study of the cirrhotic liver: Utility of administering Gd-DTPA as a complement to examinations in which SPIO liver uptake and distribution alterations (SPIO-LUDA) are present and in the identification and characterisation of focal lesions. *Radiol Med* 2006; 111:1087-1102.
- [76] Hughes-Cassidy F, Chavez AD, Schlang A, et al. Superparamagnetic iron oxides and low molecular weight gadolinium chelates are synergistic for direct visualization of advanced liver fibrosis. *J Magn Reson Imaging* 2007;26:728-737.
- [77] Aguirre DA, Behling CA, Alpert E, et al. Liver fibrosis: noninvasive diagnosis with double contrast material enhanced MR imaging. *Radiology* 2006;239:425-437.
- [78] Fischer MA, Donati OF, Reiner CS, et al. Feasibility of semiquantitative liver perfusion assessment by ferucarbotran bolus injection in double-contrast hepatic MRI. *J Magn Reson Imaging* 2012;36:168-176.
- [79] Helmberger T, Semelka RC. New contrast agents for imaging the liver. *Magn Reson Imaging Clin N Am* 2001;9(4):745-766.
- [80] Naganawa S, Kawai H, Fukatsu H, et al. Diffusion-weighted imaging of the liver: technical challenges and prospects for the future. *Magn Reson Med Sci* 2005;4:175-186.
- [81] Le Bihan D. Molecular diffusion nuclear magnetic resonance imaging. *Magn Reson Q* 1991;7:1-30.
- [82] Girometti R, Furlan A, Bazzocchi M, et al. Diffusion-weighted MRI in evaluating liver fibrosis: a feasibility study in cirrhotic patients. *Radiol Med* 2007;112:394-408.

- [83] Koinuma M, Ohashi I, Hanafusa K, Shibuya H. Apparent diffusion coefficient measurements with diffusion-weighted magnetic resonance imaging for evaluation of hepatic fibrosis. *J Magn Reson Imaging* 2005;22:80-85.
- [84] de Bazelaire CM, Duhamel GD, Rofsky NM, Alsop DC. MR imaging relaxation times of abdominal and pelvic tissues measured in vivo at 3.0 T: preliminary results. *Radiology* 2004;230:652-659.
- [85] Okada Y, Ohtomo K, Kiryu S, Sasaki Y. Breath-hold T2-weighted MRI of hepatic tumors: value of echo planar imaging with diffusion-sensitizing gradient. *J Comput Assist Tomogr* 1998; 22:364-371.
- [86] Hussain SM, De Becker J, Hop WC, et al. Can a single shot black-blood T2-weighted spin-echo echo-planar imaging sequence with sensitivity encoding replace the respiratory-triggered turbo spin-echo sequence for the liver? An optimization and feasibility study. *J Magn Reson Imaging* 2005;21:219-229.
- [87] Taouli B, Koh DW. Diffusion-weighted MR Imaging of the Liver. *Radiology* 2010;254:47-66.
- [88] Taouli B, Tolia AJ, Losada M, et al. Diffusion weighted MRI for quantification of liver fibrosis: preliminary experience. *AJR Am J Roentgenol* 2007; 189:799-806.
- [89] Kim T, Murakami T, Takahashi S, et al. Diffusion-weighted single-shot echoplanar MR imaging for liver disease. *AJR Am J Roentgenol* 1999;173:393-398.
- [90] Girometti R, Furlan A, Esposito G, et al. Relevance of b-values in evaluating liver fibrosis: a study in healthy and cirrhotic subjects using two single-shot spin-echo echo-planar diffusion-weighted sequences. *J Magn Reson Imaging* 2008;28:411-419.
- [91] Kovač JD, Daković M, Stanisavljević D, et al. Diffusion-weighted MRI versus transient elastography in quantification of liver fibrosis in patients with chronic cholestatic liver diseases. *Eur Radiol* 2011;17 [Epub ahead of print].
- [92] Luciani A, Vignaud A, Cavet M, et al. Liver cirrhosis: intravoxel incoherent motion MR imaging – pilot study. *Radiology* 2008;249:891-899.
- [93] Lewin M, Poujol-Robert A, Boelle PY, et al. Diffusion-weighted magnetic resonance imaging for the assessment of fibrosis in chronic hepatitis C. *Hepatology* 2007;46:658-665.
- [94] Sandrasegaran K, Akşık FM, Lin C, et al. Value of diffusion-weighted MRI for assessing liver fibrosis and cirrhosis. *AJR Am J Roentgenol* 2009;193:1556-1560.
- [95] Bakan AA, Inci E, Bakan S, et al. Utility of diffusion-weighted imaging in the evaluation of liver fibrosis. *Eur Radiol* 2012;22:682-687.
- [96] Manduca A, Oliphant TE, Dresner MA, et al. Magnetic resonance elastography: non-invasive mapping of tissue elasticity. *Med Image Anal* 2001;5:237-254.

- [97] Kruse SA, Smith JA, Lawrence AJ, et al. Tissue characterization using magnetic resonance elastography: preliminary results. *Phys Med Biol* 2000;45:1579-1590.
- [98] Huwart L, Peeters F, Sinkus R, et al. Liver fibrosis: non-invasive assessment with MR elastography. *NMR Biomed* 2006;19:173-179.
- [99] Rouviere O, Yin M, Dresner MA, et al. MR elastography of the liver: preliminary results. *Radiology* 2006;240:440-448.
- [100] Klatt D, Asbach P, Rump J, et al. In vivo determination of hepatic stiffness using steady-state free precision magnetic resonance elastography. *Invest Radiol* 2006;41:841-848.
- [101] Talwalkar JA, Yin M, Fidler JL, et al. Magnetic resonance imaging of hepatic fibrosis: emerging clinical applications. *Hepatology* 2008;47:332-342.
- [102] Yin M, Talwalkar JA, Glaser KJ, et al. Assessment of hepatic fibrosis with magnetic resonance elastography. *Clin Gastro Hep* 2007;5:1207-1213.
- [103] Wang Y, Ganger DR, Levitsky J, et al. Assessment of chronic hepatitis and fibrosis: comparison of MR elastography and diffusion-weighted imaging. *AJR Am J Roentgenol* 2011;196:553-561.
- [104] Huwart L, Sempoux C, Salameh N, et al. Liver fibrosis: noninvasive assessment with MR elastography versus aspartate aminotransferase-to-platelet ratio index. *Radiology* 2007;245:458-466.
- [105] Rustogi R, Horowitz J, Harmath C, et al. Accuracy of MR Elastography and Anatomic MR Imaging Features in the Diagnosis of Severe Hepatic Fibrosis and Cirrhosis. *J Magn Reson Imaging* 2012;35:1356-1364.
- [106] Annet L, Materne R, Danse E, et al. Hepatic flow parameters measured with MR imaging and Doppler US: correlations with degree of cirrhosis and portal hypertension. *Radiology* 2003;229:409-414.
- [107] Materne R, Smith AM, Peeters F, et al. Assessment of hepatic perfusion parameters with dynamic MRI. *Magn Reson Med* 2002;47:135-142.
- [108] Van Beers BE, Materne R, Annet L, et al. Capillarization of the sinusoids in liver fibrosis: noninvasive assessment with contrastenhanced MRI in the rabbit. *Magn Reson Med* 2003;49:692-699.
- [109] Hagiwara M RH, Lee VS, Losada M, et al. Advanced liver fibrosis: diagnosis with 3D whole liver perfusion MR imaging initial experience. *Radiology* 2008;246:926-934.
- [110] Thng CH, Koh TS, Collins DJ, Koh DM. Perfusion magnetic resonance imaging of the liver. *World J Gastroenterol* 2010;16:1598-1609.
- [111] Hagiwara M RH, Lee VS, Losada M, et al. Advanced liver fibrosis: diagnosis with 3D whole liver perfusion MR imaging initial experience. *Radiology* 2008;246:926-934.

- [112] Laporq B, Dumortier J, Pilleul F, Beuf O. 3D-Liver Perfusion MRI With the MS-325 Blood Pool Agent: A Noninvasive Protocol to Asses Liver Fibrosis. *J Magn Reson Imaging* 2012;35:1380-1387.
- [113] Chen BB, Hsu CY, Yu CW, et al. Dynamic contrast-enhanced magnetic resonance imaging with Gd-EOB-DTPA for the evaluation of liver fibrosis in chronic hepatitis patients. *Eur Radiol* 2012;22:171-180.
- [114] Chandarana H, Taouli B. Diffusion and perfusion imaging of the liver. *Eur J Radiol* 2010;76:348-358.
- [115] Khan SA, Cox IJ, Hamilton G, Thomas HC, Taylor-Robinson SD. In vivo and in vitro nuclear magnetic resonance spectroscopy as a tool for investigating hepatobiliary disease: a review of H and P MRS applications. *Liver Int* 2005;25:273-281.
- [116] Solga SF, Horska A, Clark JM, Diehl AM. Hepatic 31P magnetic resonance spectroscopy: a hepatologist's user guide. *Liver Int* 2005;25:490-500.
- [117] Khan SA, Cox IJ, Hamilton G, Thomas HC, Taylor-Robinson SD. In vivo and in vitro nuclear magnetic resonance spectroscopy as a tool for investigating hepatobiliary disease: a review of H and P MRS applications. *Liver Int* 2005;25:273-281.
- [118] Johnson NA, Walton DW, Sachinwalla T et al. Noninvasive assessment of hepatic lipid composition: advancing understanding and management of fatty liver disorders. *Hepatology* 2008;47:1513-23.
- [119] Cobbold JF, Anstee QM, Goldin RD et al. Phenotyping murine models of non-alcoholic fatty liver disease through metabolic profiling of intact liver tissue. *Clin Sci* 2009;116:403-13.
- [120] Cobbold JF, Patel JH, Goldin RD et al. Hepatic lipid profiling in chronic hepatitis C: an in vitro and in vivo proton magnetic resonance spectroscopy study. *J Hepatol* 2010;52:16-24.
- [121] Lok AS, Everhart JE, Chung RT, et al. Evolution of hepatic steatosis in patients with advanced hepatitis C: results from the hepatitis C antiviral long-term treatment against cirrhosis (HALT-C) trial. *Hepatology* 2009;49:1828-1837.
- [122] McPherson S, Jonsson JR, Cowin GJ, et al. Magnetic resonance imaging and spectroscopy accurately estimate the severity of steatosis provided the stage of fibrosis is considered. *J Hepatol* 2009;51:389-397.
- [123] Georgoff P, Thomasson D, Louie A, et al. Hydrogen-1 MR Spectroscopy for Measurement and Diagnosis of Hepatic Steatosis. *AJR Am J Roentgenol* 2012;199:2-7.
- [124] Noren B, Dahlqvist O, Lundberg P, et al. Separation of advanced from mild fibrosis in diffuse liver disease using 31P magnetic resonance spectroscopy. *Eur J Radiol* 2008;66:313-320.

- [125] Taylor-Robinson SD. Applications of magnetic resonance spectroscopy to chronic liver disease. *Clin Med* 2001;1:54-60.
- [126] Lim AK, Patel N, Hamilton G, et al. The relationship of in vivo 31P MR spectroscopy to histology in chronic hepatitis C. *Hepatology* 2003;37:788-794.
- [127] Sijens PE, Oudkerk M. Clinical magnetic resonance spectroscopy. *Imaging Decisions MRI* 2005;9:23-38.
- [128] Wang QB, Zhu H, Liu HL, Zhang B. Performance of Magnetic Resonance Elastography and Diffusion-Weighted Imaging for the Staging of Hepatic Fibrosis: A Meta-Analysis. *Hepatology* 2012;56:239-247.
- [129] Godfrey EM, Patterson AJ, Priest N, et al. A comparison of MR elastography and 31P MR spectroscopy with histological staging of liver fibrosis. *Eur Radiol* 2012 [Epub ahead of print].